

ResNet and CWT Fusion: A New Paradigm for Optimized Heterogeneous Thin Reservoir Evaluation

Saima Akram,* Gulraiz Akhter, Yonggang Ge, and Tahir Azeem

Cite This: *ACS Omega* 2024, 9, 4775–4791

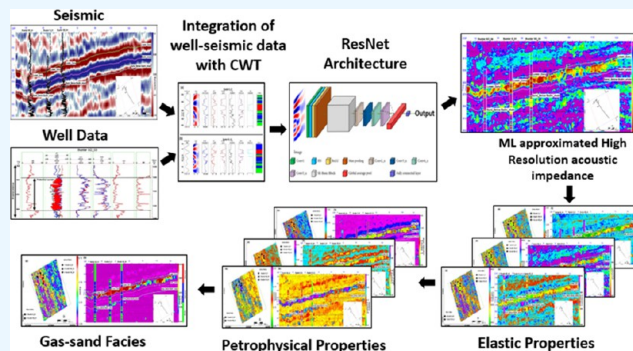
Read Online

ACCESS |

Metrics & More

Article Recommendations

ABSTRACT: The endeavor to explore and characterize oil and gas reservoirs presents significant challenges due to the inherent heterogeneities that are further compounded by the existence of thin sand layers encapsulated in shale strata. This complexity is intensified by limited and low-resolution seismic data, missing critical well-log information, and inaccessible angle stack data. Conventional reservoir classification approaches have struggled to address these issues, primarily due to their limitations in handling missing data effectively and, hence, precise estimations. This study focuses on the characterization of thin, heterogeneous potential sands of the B-interval within the Lower Goru Formation, a proven gas reservoir in the Badin area. The reservoir sands with varying thicknesses are assessed in detail for their optimized description and field productions by handling challenges, including low seismic resolutions, heterogeneities, and missing data sets. An innovative solution is developed based on the integration of continuous wavelet transform (CWT) and machine learning (ML) techniques for the approximation of missing data sets, i.e., S-wave (DTS), along with enhanced elastic and petrophysical properties. The improved properties are augmented by the high resolution attained by CWT and captured variability more profoundly through the implication of residual neural networks (ResNet). The limitations of conventional approaches are harnessed by ML solutions that operate with limited input data and deliver significantly improved results in characterizing enigmatic thin sand reservoirs. The high-frequency petroelastic properties reliably determined the thin heterogeneous potential sand bodies and illuminated a channelized play fairway that can be tested for additional wells with low-risk involvement.



1. INTRODUCTION

The complex interlayers of sands and shales within the Lower Goru Formation (LGF) are predominantly the result of changing sediment influx and diverse depositional environments.¹ The heterogeneous reservoir sand intervals of the LGF exhibit varying thicknesses ranging from 20 to 35 m, which is notably below the resolution capabilities of traditional seismic imaging techniques. The high heterogeneity, limited and low-resolution seismic data, missing DTS, and inaccessible angle stack data add challenges to reliably characterizing these thin reservoir sand intervals. As the LGF has demonstrated promising production in certain wells, its characterization and proper imaging are essential for the enhanced recovery from the producing field.

Initially, conventional approaches, including seismic interpretation,² petrophysical assessments,³ and fault-seal analysis,⁴ have been done in the research area. Additionally, meticulous approaches like deterministic and stochastic seismic inversions have been employed in various nearby producing fields to tackle these challenges.^{5–7} However, their effectiveness in such complex geological settings often falls short, primarily due to their inability to handle missing data effectively, and the

increased number of procedural steps may cause uncertainty. In recent years, the comparable use of advanced ML techniques has gained significant interest in subsurface imaging and reservoir characterization due to their enhanced result, robustness, and efficiency.⁸ A comprehensive solution has been developed, focused on an integrated strategy that combines different types of data along with various approaches (petrophysics, rock physics, and seismic inversion) and employs modern ML algorithms to successfully handle reservoir challenges.

The available P-wave velocity (DTP) and density (RHOB) proved valuable for subsurface characterization, but the absence of DTS poses challenges and limitations in fully understanding the subsurface facies. The conventional

Received: October 20, 2023
Revised: December 16, 2023
Accepted: December 20, 2023
Published: January 12, 2024



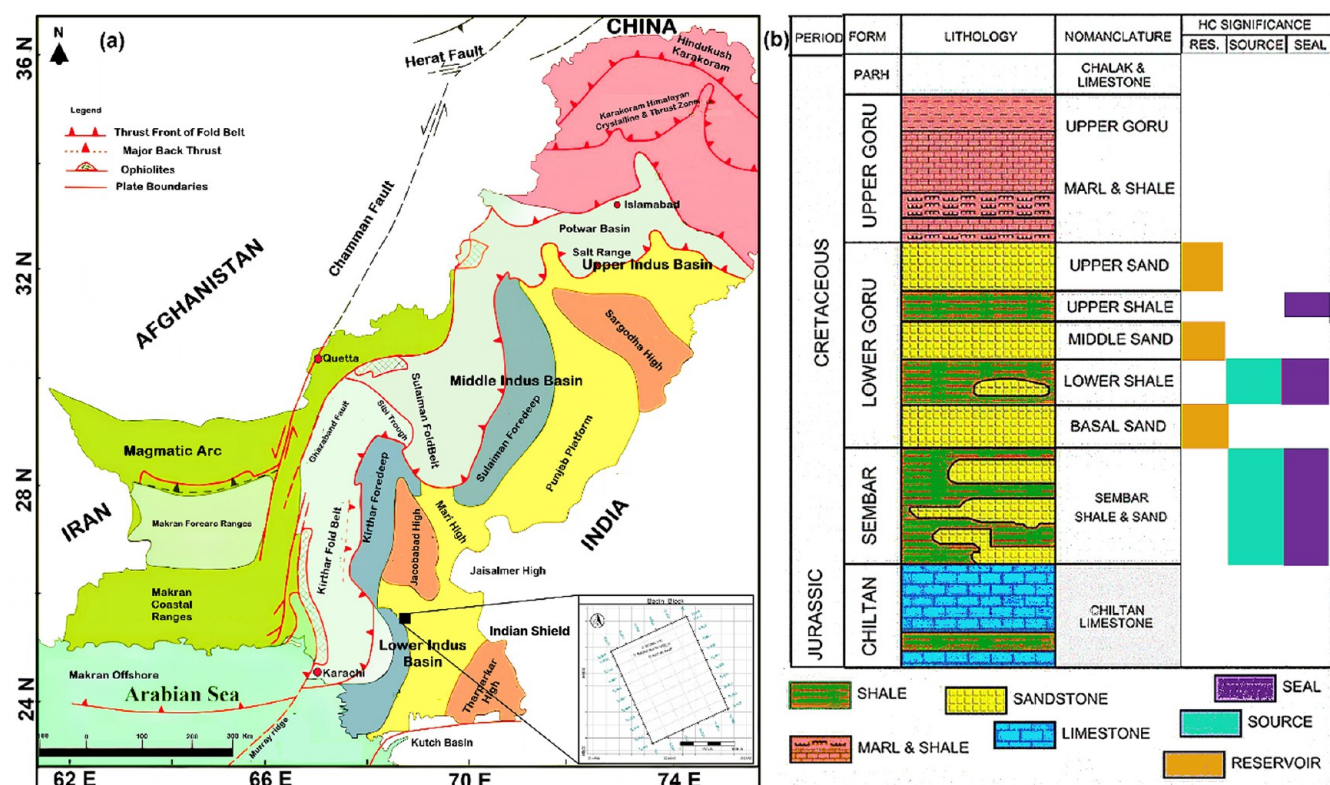


Figure 1. (a) Regional map depicting structural elements (modified after Kazmi and Sneek⁴⁵ and study area and (b) stratigraphic chart illustrating the petroleum system with a major source, reservoir, and seal.^{33,46}

techniques have been employed by numerous researchers previously for the prediction of DTS within the producing fields both locally⁹ and globally.¹⁰ Conversely, a number of researchers have recently used ML techniques for predicting the DTS curve with success.^{8,11–14} ML techniques have been developed for their robustness to address technical problems like wellbore's unrecorded logs or discrepancies along measured logs based on analyzing and training consistent well properties.¹³ Noise-free data form the foundation for optimized results in ML, while noisy or limited point sets were eliminated from the measured logs before training using a designated model. The ML is comprehensively performed on selected logs employed for the estimation of DTS, including DTP, RHOB, volume of shale (Vsh), effective porosity (PHIE), and water saturation (Sw), which provided a reasonable improvement in comparison with empirically derived DTS at well using Castagna's equation.

The complex reflection pattern from thin beds generates tuning effects and deteriorates the seismic amplitudes, obscuring the precise low-frequency shadow zone of the reservoir. The spectral decomposition (SD) technique is widely employed to decompose frequency contents of various signals in the time–frequency domain. The CWT of the SD technique proves to be more effective in distinguishing hydrocarbon-bearing reservoirs with varying thicknesses, including both thin- and thick-bedded layers when compared to the limited frequency range of seismic characteristics.¹⁵ It identifies thin beds at a resolution of 1/4th of the wavelength of the dominant period by the detection of extreme magnitude response within the specified frequency range.^{16–19} The CWT proved efficient in many fields, including Lakshmi field, elucidating the channel morphology and forecasting the gross

sand thickness that amplitude-based methods could not achieve.²⁰ The CWT's efficiency offered high-frequency resolution comparatively to the short-time Fourier transform (STFT) for identifying the hydrocarbon reserves²¹ as it can record more accurately the delicate variations in frequencies arising from the presence of hydrocarbons.^{22–25} In the past few years, scholars approved the CWT application along with the seismic inverted properties for the stratal inquiries of the diverse reservoirs and evaluation of hydrocarbon capabilities. The inverted characteristics (P-impedance, S-impedance, V_p/V_s ratio, etc.) have significantly proven their worth in distinguishing fluids as well as the lithological components of the reservoir. The probabilistic neural network (PNN), a nonlinear interpolation associated with pattern recognition, utilizes multiattributes of wells and seismic properties (impedances, V_p/V_s ratio, etc.),²² to better manage shales inside sands and petrophysical distributions.^{23,24}

The spatial variability is exceptionally assessed for enhanced reservoir characterization by employing CWT along with inverted attributes obtained through Residual Network (ResNet), a deep neural network technique (DNN).³² Artificial intelligence can now be used to improve the precision and resolution of subsurface property calculations after the development of ResNet for image recognition tasks on seismic and well-log data.³³ Overall, in this integrated approach, ResNet has played a central role in tackling the complexities of heterogeneous reservoirs and thin sand beds on the CWT components of seismic trace (real, imaginary, magnitude). Its ability to train DNN effectively, while mitigating common ML challenges, positions ResNet as a superior choice for capturing intricate relationships between CWT seismic components and identified facies.²⁷ ResNet obtained impressive importance in

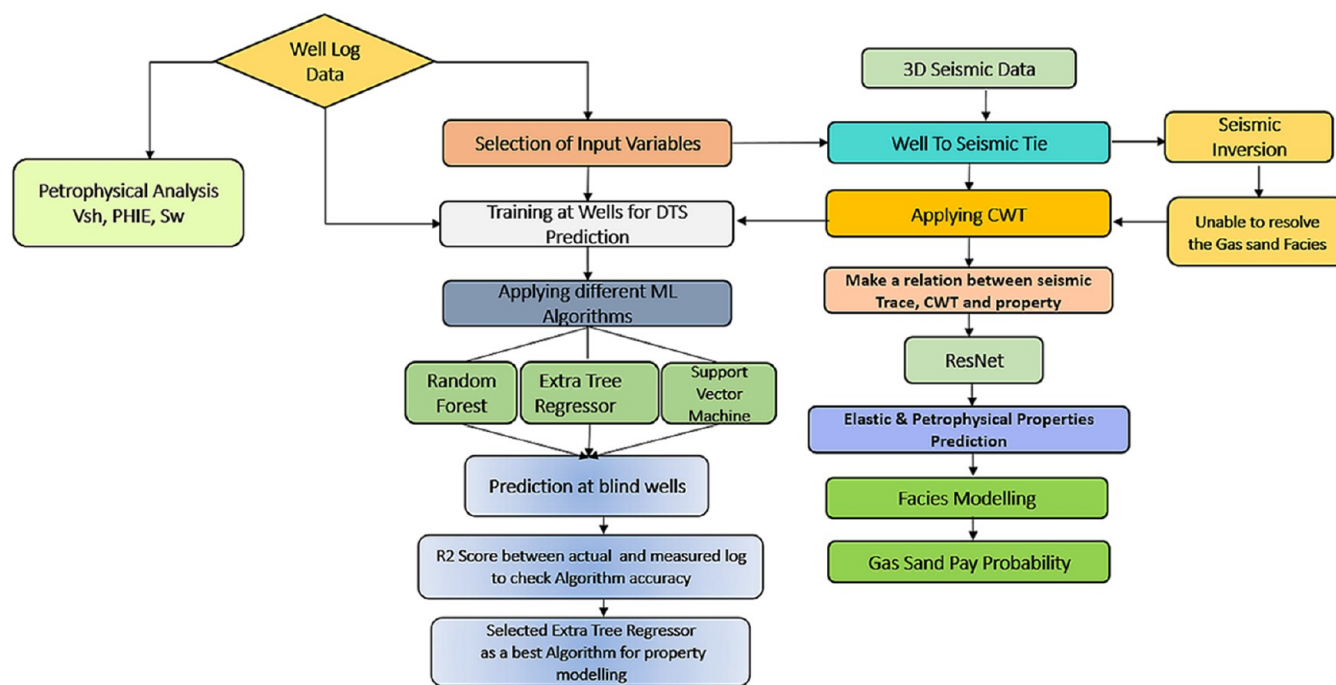


Figure 2. Complete workflow for the prediction of missing DTS and the estimation of petrophysical and elastic properties for the enhanced characterization of thin heterogeneous sands, integrating CWT and ResNet algorithms.

advancing the field of deep learning (DL) by incorporating image identification, natural language processing, and machine translation^{28,29} while alleviating issues like resilient to noise and overfitting, vanishing gradients, and being more efficient and less computationally expensive to train.^{30–32}

The thin potential sands within the LGF have remained a challenging puzzle in the field of reservoir characterization in the Badin area, with no prior comprehensive work or established solutions to resolve them. In the present work, the novel machine learning (ML) approach optimized the resolution limitations of approximated properties (elastic and petrophysical) and evaluated the heterogeneities of reservoir sands more comprehensively. The ML solutions employing limited input data delivered significantly improved results and highlighted channelized potential sands more pronouncedly compared to traditional methods.

2. GEOLOGY AND STRATIGRAPHY OF THE AREA

The Indus Basin (IB) is the biggest onshore sedimentary basin of Pakistan, located to the northwest of the Indian Shield.³³ Based on structural makeup and potential for petroleum, the IB is alienated into three sub-basins, i.e., upper, middle, and lower.³⁴ The Upper Indus Basin (UIB) exhibits a compressional regime and is quite active tectonically, whereas the Lower Indus Basin (LIB) lies in an extensional regime and is relatively less active.^{35,36} During the Cretaceous period, tectonic activity in the Indus Basin formed a rift zone, which marked the beginning of the procedure that controlled the depositional system within the LIB.³⁵ The horst and graben structures were caused by the late Cretaceous rifting that occurred between India and the Seychelles.³³ During this period, the rate of spreading was rapid, ranging from 20 to 30 cm/a.^{35,37}

The Badin region is situated in the eastern portion of the LIB and is characterized by normal faulting in the region (Figure 1a). It is bounded by the Indian Shield on the east, the

Kirthar Fold and Thrust Belt to the west, and Jacobabad high to the north.^{1,38} The rate of deformation in the Badin region is comparatively small because of its distance from the primary tectonic zone.³⁹ Within the Sindh monocline, the Badin area has the highest success rate in terms of oil and gas exploration.³⁸ The reservoir in the Badin area is bounded by normal faults providing a lateral seal for the hydrocarbons.^{35,40}

The Cretaceous LGF is formed in a shallow marine environment and provides important information about the sea-level changes and the evolution of marine life during this period.^{41,42} The formation is associated with westerly prograding river-dominated deltas that were created by river systems that drained through the Indian Shield from the east and southeast. The B-sand interval of the Lower Goru Formation exhibits considerable heterogeneity as a consequence of the different depositional environments on the proximal and distal sides.⁴³ Grain size variability within the formation is created by the transition from coarse to fine sediments.⁴⁴ These differences affect the rock's permeability and porosity, which affects fluid movement in subsurface reservoirs. The interbedded shales between reservoir sands of the LGF act as a seal, while the Sembar shales are the dominant source in this area (Figure 1b).

3. MATERIALS AND METHODS

In this research, 3D seismic poststack and wireline logging data, e.g., γ -ray (GR), spontaneous potential (SP), DTP, DTS, RHOB, neutron porosity (NPHI), deep resistivity (LLD), and shallow resistivity (LLS), have been incorporated using three wells (Buzdar S_01, Buzdar SD_03, Buzdar SD_04). Well reports of two blind wells, Buzdar S_02 and Buzdar SD_01, were also used. The target reservoir is hit by the three wells employed in the study lying with the 3D seismic cube. Key information regarding formation tops, mineralogical properties, and physical characteristics of the reservoir were assimilated to generate a relationship between elastic and petrophysical

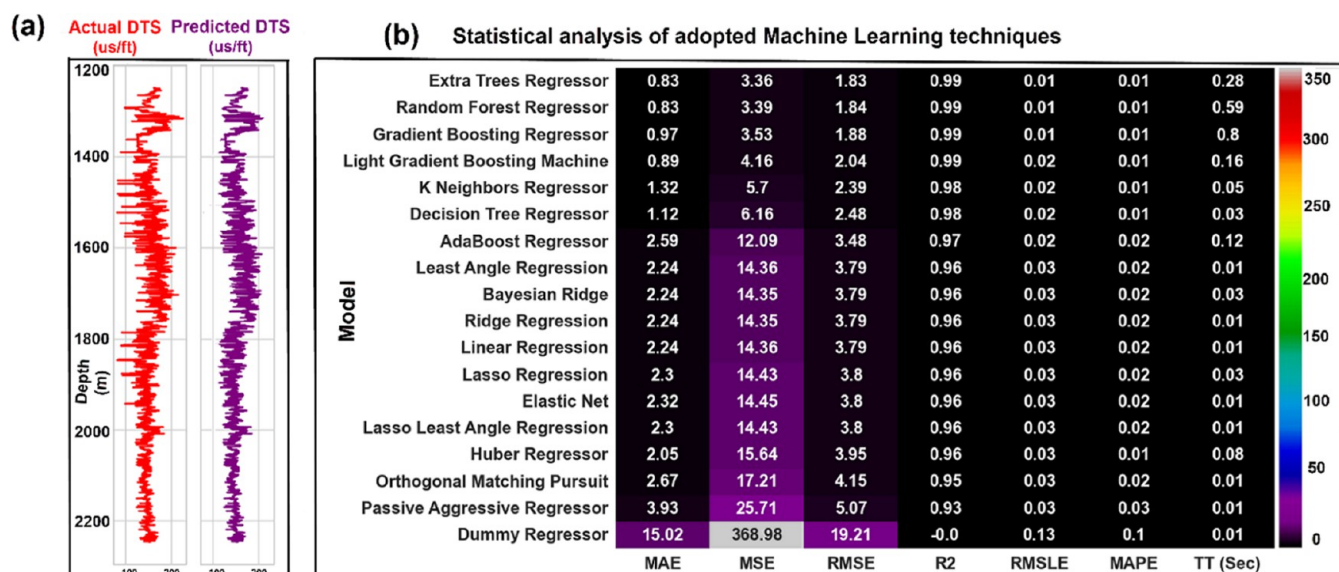


Figure 3. (a) Measured DTS (red) and modeled DTS (purple) () delineated a good matching of trends and values. (b) Statistical analysis of the adopted ML techniques depicted the performance of each algorithm employed for the prediction of DTS.

properties. The measured data quality regarding well logs was fair, except for certain problems included during recording. For instance, the RHOB was conceded in wells due to borehole conditions, such as washout, while DTS was not recorded in any of the wells. Such limitations hindered the reliable approximations of reservoir properties; therefore, advanced techniques were employed to handle the discrepancy in the data set and estimate the thin heterogeneous profoundly. Figure 2 shows the complete methodology adopted in this research.

Starting with the analysis of well logs and seismic data, a reliable seismic correlation is established and three horizons from top to bottom, i.e., LGF, Badin shale, and Sand below Badin shale, are subsequently mapped to determine their spatial extent. The seismic data's vertical resolution is less than potential sand bed thicknesses, which is determined by the $\lambda/4$ th i.e., one-fourth of the trace wavelength.⁴⁹ The observed seismic data peak frequency is 20 Hz and the reservoir sand interval velocity is 2650 m/s, hence depicting a maximum resolution up to 47 m, proving the tuning of thin-bedded potential sands at various locations throughout the field.⁵⁰ Hence, band-limited seismic along with its inverted properties with limited vertical resolution would be incapable of producing credible results for comprehensive reservoir characterization. Therefore, advanced ML approaches are used to resolute thin pay sand beds with varying reservoir thicknesses averaging 20–35 m in the present study.⁴⁷

Conventional rock physics modeling (RPM) is carried out for multiple purposes, including the assessment of heterogeneities, detailed reservoir characterization, and predicting missing logs, mainly DTS.^{5,7,8,25,52} The consistent and improved modeled DTS log was further utilized in seismic inversion techniques for upgraded reservoir characterization. Log data limitations of the IB, including poor RHOB along with the absence of DTS, are assessed using traditional RPM, incorporating petrophysical results, in situ parameters of the reservoir, and integration of petroelastic attributes.

Despite the consistent results of RPM, the requirements of interdependent processes make it highly subjective, because if any error ascends it glides toward the outcome. Contrarily, ML

seemed as an effective tool having the capacity to develop a direct link among log curves based on their prominent features; hence, robust and reliable predictions of missing or poor logs are made for comprehensive assessment of reservoir characteristics. ML techniques have been recently employed for the estimation of DTS by engaging test and training data sets.^{9,10,12} ML is developed as an advanced approach for handling practical complications, primarily related to unmeasured logs or shortages within measured logs by examining, testing, and training reliable logs.¹³ The algorithms of supervised machine learning (SML), an elementary method of ML, generate a model for associating data (or feature) vectors to a corresponding label or target vector using training data. The combination of input and its connected labels are recognized and incorporated into the procedure.⁴⁸ The modeling of logs or their improvement acts as a basic part of the regression model employed for forecasting the continuous numerical variables.¹³ The wells providing logs for predicting DTS in a similar well are termed test data, whereas the remaining wells involved in the process are called training data. Various SML techniques, including random forest (RF), decision tree regressor (DTR), extended tree regressor (ETR), multiple and support vector machine (SVR), etc., were incorporated for training the data set (seismic and well), selecting the best technique based on evaluation metrics, and further employed to extract elastic and petrophysical attributes. The best method assessed for DTS prediction based on the statistical analysis is ETR, which develops a comprehensive relation with seismic trace components extracted through CWT for the final prediction of petroelastic properties.

The modeling of corresponding logs due to washouts along with measuring of logs in splice zones is a fundamental step in the characterization of rock strata employed in petrophysical properties estimation.⁴⁹ The modeling of missing logs was carried out after the removal of outliers and qualitative review of input data. In the present research, the SML technique was adopted for improving the measured log models. The DTS curve was not available in any well, so it was initially derived from Castagna's empirical relationship using measured p-wave. Therefore, DTS is predicted by finding an association with

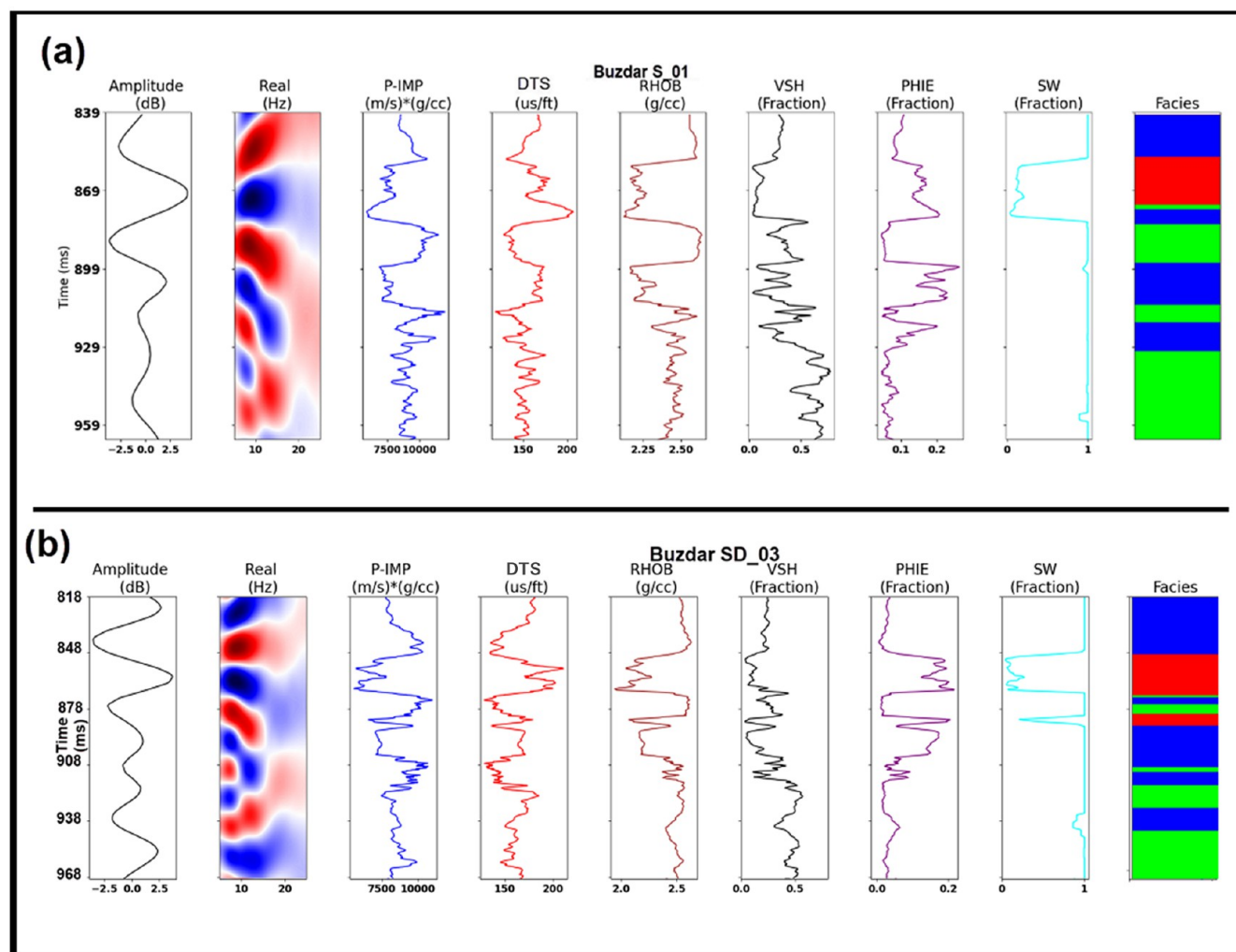


Figure 4. Petro and elastic properties of wells (a) Buzdar S_01 and (b) Buzdar SD_03 integrated with the real part of the seismic (decomposed by CWT) along with usage of ResNet for predicting the petroelastic volumetric approximation. The facies probability is the final achievement with net/gross thickness estimated through cutoffs i.e., $V_{sh} < 30\%$, $PHIE > 5\%$, and $Sw < 45\%$.

recorded logs using advanced ML techniques. The empirically approximated DTS by Castagna's relationship is utilized in the training procedures through many significant processes (RF, DTR, SVR, and others), as shown in Figure 3a, for Buzdar S_01. The unrecorded DTS was approximated in all of the remaining wells by utilizing the aforementioned ML techniques. To validate the implemented methodology regarding DTS estimation, the modeled DTS of Buzdar S_01 was shared for the prediction of DTS in Buzdar SD_04 wells while keeping the measured DTS curve blind in the Buzdar SD_03 well. ML worked on improved logs by dividing the data by 60% training and 40% testing. This testing and training are changed randomly for each iteration.

The finest ML techniques are recognized by the evaluation metrics established on various samples extracted from training, including mean average error (MAE), mean square error (MSE), root mean square error (RMSE), root mean square least error (RMSLE), correlation coefficient (R2), mean absolute percentage error (MAPE), and training time (TT). Helpful values regarding the analyzed indicators suggested that the model is probably operating more effectively.⁵⁰ It was observed that ETR proved to be the most effective ML technique for estimating the unrecorded DTS with a maximum

R2 score of 0.99, a low MSE of 3.36, least TT of 0.28 sec. and an RMSE of 1.83, accompanied by additional helpful statistical measures (Figure 3b). The predicted DTS along with elastic and petrophysical properties on decomposed seismic with CWT (real part of seismic trace) is employed for volumetric estimation through ResNet to accomplish the aforementioned limitations.

3.1. Continuous Wavelet Transform. The CWT algorithm within SD is widely employed, regarding the decomposition of strata layers along with the analysis of their compositional attributes.⁵¹ This transformation is also referred to as frequency-dependent SD, as it breaks down the traditional time-domain amplitudes into their frequency-domain counterparts.⁵² Consequently, the isofrequency panels provide a clear representation of how time-domain amplitudes have been decomposed to frequency domain, a crucial aspect of the current study. It operates by adjusting the time support of the wavelets to accommodate diverse frequencies. Once the time support expands or contracts, the frequency assistance of the wavelet shifts toward higher or lower ranges of frequency, respectively. Consequently, the resolution of the frequency improves while the resolution in time diminishes, and vice versa.⁵³ CWT conveys remarkably improved vertical seismic

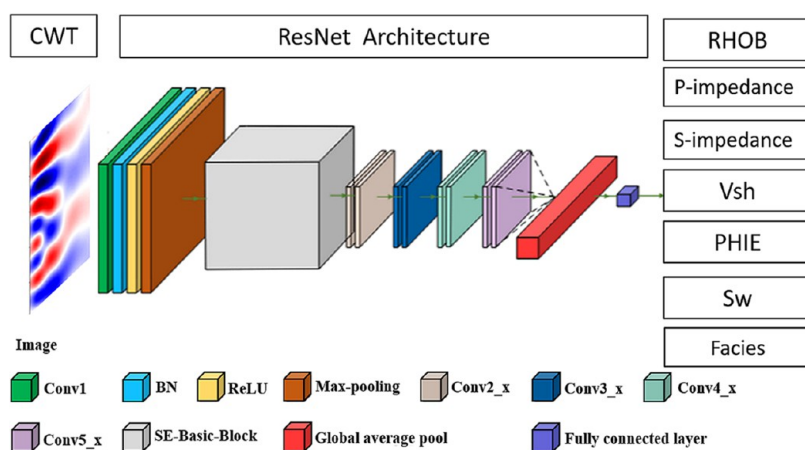


Figure 5. Architecture of the proposed ResNet model represents major components and layers with ultimate results.

resolution when observed as a repeated panel of a nonstationary seismic signal. CWT offers precise characterization of stratigraphic reservoirs within the time–frequency domain, ultimately delivering the finest vertical seismic resolutions.^{54,55}

The basic methodology comprises that CWT decomposes the signal by convolving it with the wavelet.⁵⁶ These wavelets are scaled and translated to cover all possible scales and positions and are then correlated with the signal. This correlation provides information about the presence of features or patterns in the signal on that particular scale and position. CWT reduces the number of data points in the transformed signal to focus on specific frequency components by selecting certain scales or frequencies of interest and discarding others, which allows preservation of high-frequency components.⁵⁷ A complex-valued signal is obtained as a result of CWT, which has both real and imaginary parts.⁵² The real part of the CWT represents the amplitude of the wavelet that best matches the signal, whereas the imaginary part represents the phase information.⁵⁸ CWT analyzes the high-frequency components effectively in seismic data that are crucial for characterizing the subsurface by selecting the appropriate wavelets and scales. This preserved high-frequency information can be related to high-frequency well data, such as data from sonic logs, which are sensitive to the subsurface's elastic properties.⁵⁹ The real part of the CWT signal is trained on petrophysical properties like PHIE, Vsh, and Sw along with the elastic properties, including P-impedance, DTS, etc., which have direct effects on the amplitude of seismic waves⁶⁰ (Figure 4a,b). Assimilating seismic data and well-log data, the CWT is applied to extract features, which are then passed through the trained ResNet for prediction.⁶¹

3.2. ResNet Architecture. ResNet works on a DNN architecture having the ability to handle very deep networks successfully. It consists of several layers, including convolutional layers, residual blocks, and fully connected layers.⁶² The input to a residual block is directly incorporated into the outcome of that block. This means that the network can learn to make small adjustments to the input feature map to produce the desired output.⁶² After multiple residual blocks, a ResNet typically includes fully connected layers or other specialized layers for specific tasks like classification or regression.⁶³ The gradient can easily flow through the skip connections, making it possible to train very deep networks.⁶⁴

The ResNet model has multiple layers, including Conv1, SE-Basic-Block, Conv2_x, Conv3_x, Conv4_x, and Conv5_x, a

global average pooling layer, and a fully connected layer (Figure 5). A convolutional layer Conv1 includes a batch normalization layer, activation function ReLU, and a max-pooling layer.⁶⁵ The max-pooling layer's addition aids in minimizing the model's dimensions and parameters, expanding the receptive fields, and retaining important feature information. SE-Basic-Block is the second part and comprises a residual basic block and a squeeze-and-excitation (SE) module. There are two convolutional layers in the second part. The SE module was embedded in the residual basic block to form a SE-Basic-Block. Output features of SE-Basic-Block become inputs of Conv2_x. This feature mapping similarly continues to Conv3_x and so on up to Conv5_x. The seventh part global average pool uses the GlobalAvgPool function, and the output size of this layer is set to 1×1 . The eighth part, the fully connected layer, is the classifier of ResNet. Its output was set to 1, which corresponds to the types of data sets to train and classify, i.e., elastic, petrophysical, and gas sand facies. ResNet is trained using backpropagation with RMSprop and a learning rate of 0.0001.

The extracted features from CWT can serve as input to the ResNet architecture. Thin bed gas sand facies prediction using ResNet involves seismic data preprocessing, i.e., clean, normalize, align, handling missing values and outliers to remove noise and to extract relevant features.⁶⁶ ResNet is trained on labeled data, where the labels could represent various geological or petrophysical properties of interest, such as lithology, porosity, or fluid saturation, and split the labeled data set into training, validation, and testing subsets.²⁷ During training, ResNet learns to map the extracted features from CWT to the target properties, effectively learning the complex relationships within the data. The integration of CWT and ResNet creates an iterative framework that can be refined over time with the enhanced band of seismic data and its derived attributes.⁶⁷

Once the ResNet model is trained, it can predict various subsurface properties or classifications (elastic, petrophysical, and gas sand probability volume) based on the learned patterns, which can be critical for reservoir characterization or exploration tasks.⁶⁸ The integrated framework allows not only accurate predictions but also interpretable outputs. Overall, the integration of CWT and ResNet combines the strengths of advanced signal processing techniques with the DL capabilities. This approach can enhance the accuracy and efficiency of subsurface characterization, making it particularly valuable in

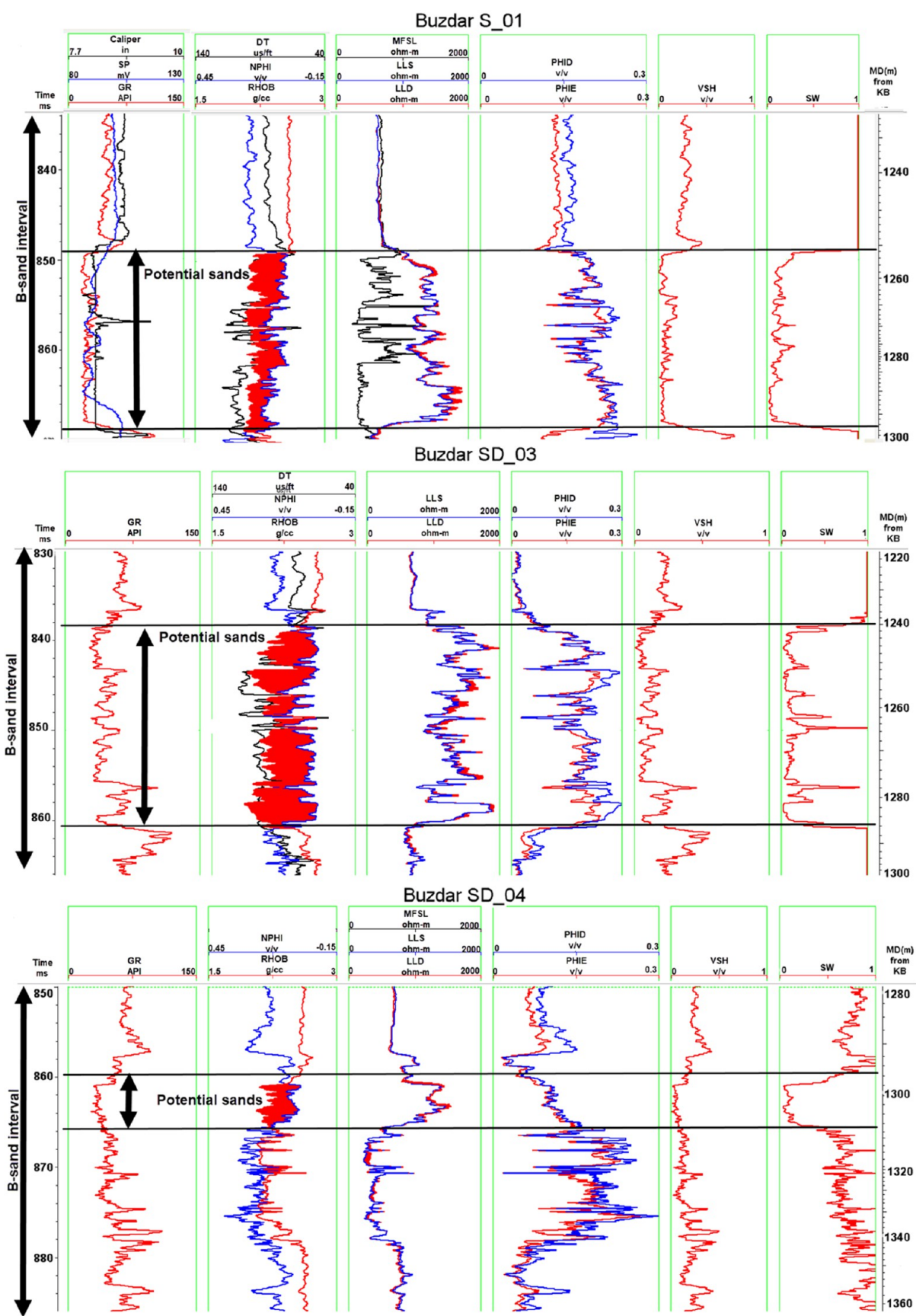


Figure 6. Petrophysical properties of all three wells: (a) Buzdar S_01 highlighted a potential body of 40 m calculated by the behavior of low GR, NPHI-RHOB crossover (filled by red), high LLD values than LLS (filled by red) with good porosity and less Sw; (b) Buzdar SD_03 depicted a potential sand body of about 50m observing similar log behavior; and (c) Buzdar SD_04 shows comparatively thin plausible zone of only 15 m.

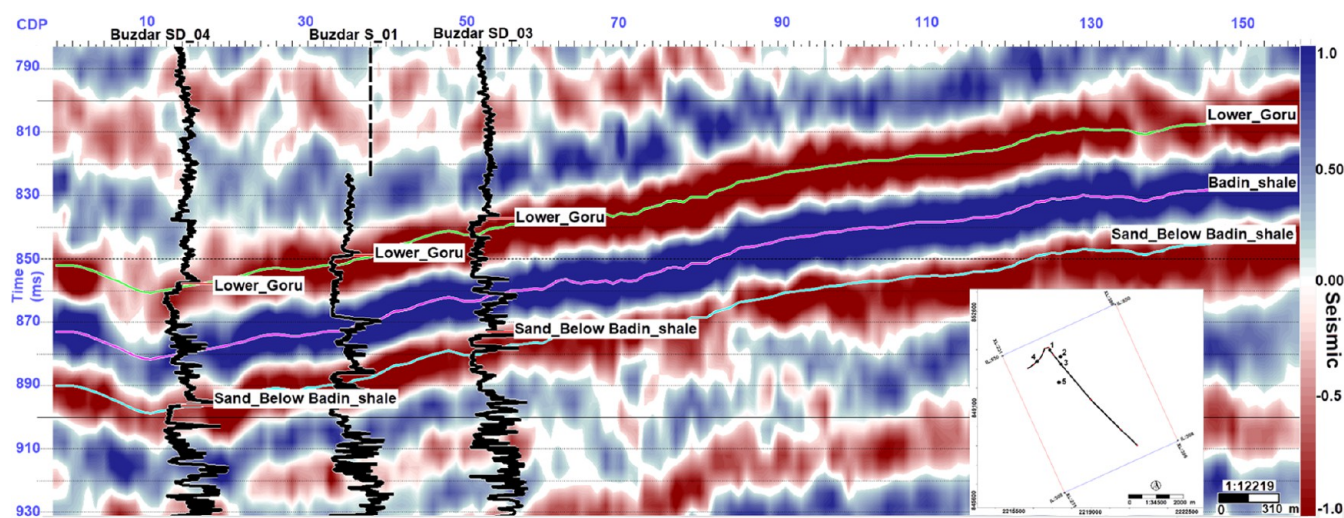


Figure 7. Interpreted seismic section on an arbitrary line passing through wells employed in the study delineates the overall trend of the interpreted horizons (dipping in the northwest direction due to basement highs in the southeast) covering the LGF. The index map shows the arbitrary line coverage in the field.

the oil and gas industry for optimizing reservoir evaluation and exploration efforts.

4. RESULTS

In the current study, many of the severe problems are handled through combined techniques, including a definite reservoir zone identification through petrophysics and stratal variation through horizon picking along with structural delineation. Also, missing data approximation and limitations in the seismic data set, such as the range of angle sets, are exceptionally handled by the implication of ML techniques. The integration of ResNet with CWT provided a solution toward more enhanced property prediction compensating for the data resolution problems. The adopted workflow starting from missing data prediction, generating high-frequency components, such as S-impedance using poststack seismic along with its CWT attributes, and then estimating petrophysical properties delineated the heterogeneity of the reservoir more profoundly. Finally, the reservoir facies are modeled through a relationship utilizing both elastic (P-impedance, S-impedance, DTS, RHOB) and petrophysical (PHIE, Vsh, Sw) properties for the demarcation of producing sand probabilities.

4.1. Petrophysics. Several processes were performed for petrophysical analysis, initiated by identifying the possible reservoir zone within the prolific B-interval. The signatures of logs are analyzed in detail to designate their potential significance. All three delineated plausible gas-bearing zones by the assessment of calculated petrophysical properties, including Vsh, porosities, and Sw. The analysis approved the presence of sands with intercalation of shales. Comparatively to the B-interval in nearby fields, such as Kadanwari, Mehar, Sawan, etc., the thickness of potential sands is good with a net thickness of about 40 m within the depth range of 1250–1290 m in Buzdar S_01 (Figure 6a). The validation of the results was confirmed by observing the NPHI-RHOB crossover, as well as the clear demarcation among the deep (LLD) and shallow (LLS) resistivity curves. The calculated reservoir properties, i.e., Vsh ranging 9–10% in the lithology track (less values demarcated clean potential sands within B-Interval), PHIE about 15–18% within the porosity track, and Sw of

approximately 8% in the saturation track, result in gas-prone sand facies delineation.

Similarly, Buzdar SD_03 is evaluated, and the gas-bearing zone within the B-interval is recognized based on the hard constraint well logs' petrophysical evaluation. The thickness of the potential body is approximately 50 m with PHIE ranges of 14–17%, Vsh is 8–10% and Sw of 8%, making it overall a clean, porous, and potential sand (Figure 6b). Buzdar SD_04 is less prominent as the producing sands' net thickness is not as much in comparison to the other interpreted two wells. The net thickness observed for the gas sand lithofacies is about 15 m within the depth range of 1295–1310 m based on the calculated properties, including Vsh of around 6–7%, PHIE estimated to be 8–15%, and less Sw of 6% (Figure 6c).

4.2. Seismic Interpretation. The formation tops of various lithologies observed during the well drilling were correlated with seismic data for interpreting horizons. Overall, three horizons have been interpreted, depicting the stratigraphical variation of beds, namely, Lower_Goru, Badin_shale, and Sand_Below Badin_shale (Figure 7). The interpreted section of an arbitrary line covering the entire field demarcated the deepening of formations in the northwest while shallower regions in the southeast due to basement high. The basement highs provided the sediment influx that is deposited westward and can be observed on flattened seismic sections by the thickening of the deposited sediments. Deposition at all levels is believed to be from the southeast to northwest direction.² The wells are drilled comparatively in deeper zones while bonded locally in the horst-graben structural styles, hence confirming the extensional regime with the normal faulting pattern. Such structures are present throughout the LIB along with basic elements of the petroleum system. Grabens are the main areas for the generation of hydrocarbons, whereas accumulation is made via horsts that trap hydrocarbons. The main constituents of the petroleum system are present as proven by the number of oil and gas discoveries in the area.²

4.3. Elastic and Petrophysical Properties. The consistent DTS is estimated using ML techniques that are furthermore employed for the prediction of S-impedance volumes using poststack seismic by the integration of ResNet and CWT. The dependency of single properties, i.e., acoustic

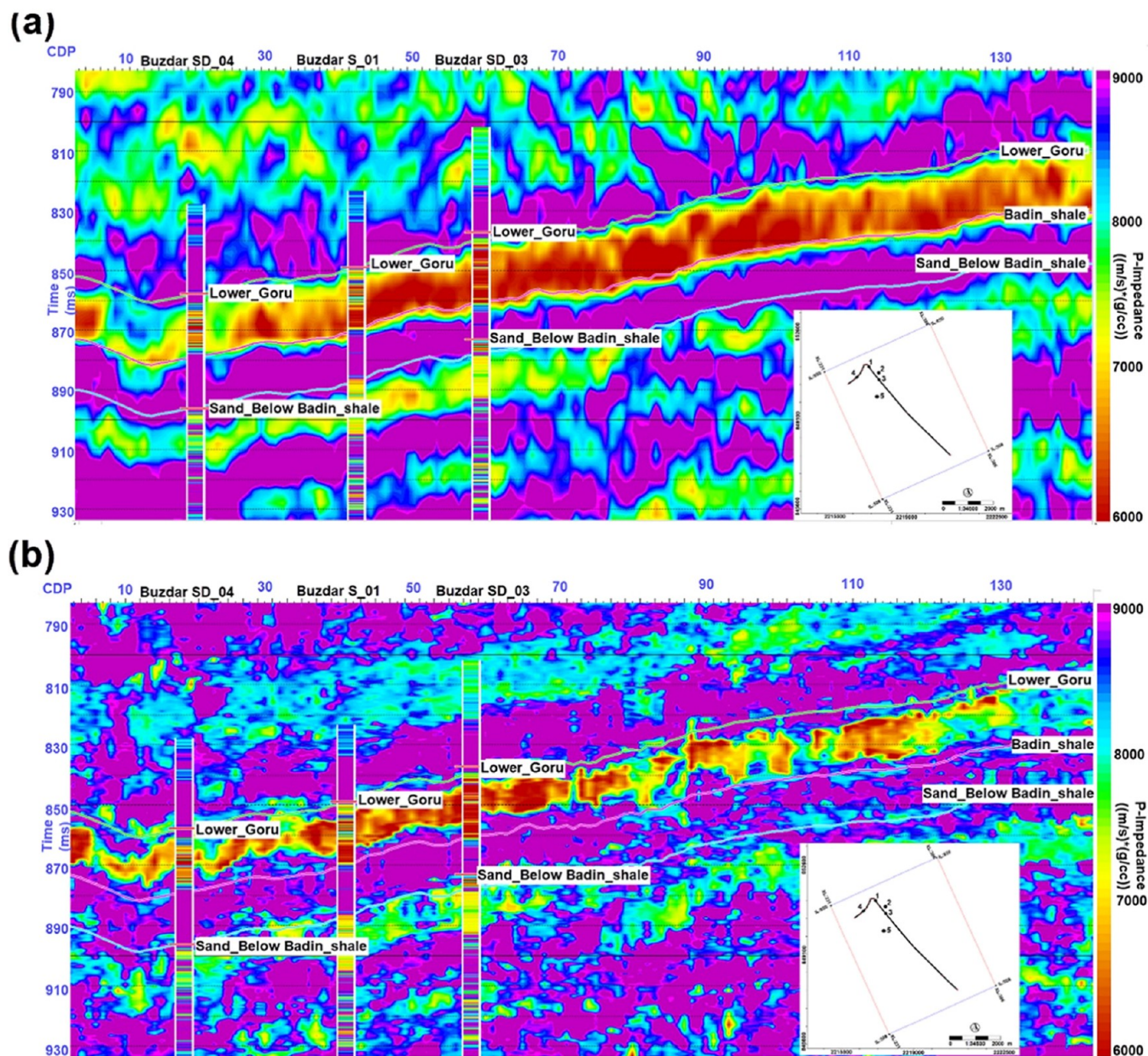


Figure 8. (a) Conventional P-impedance observing low resolution for potential sand bodies and (b) advanced ML technique improved the resolution of P-impedance with enhanced capability of illuminating heterogeneous thin potential sands.

impedance, vanished by providing additional components of seismic data along with improved resolution for characterizing thin heterogeneous sands. The conventional seismic inversion techniques offer a qualitative assessment of subsurface configurations and struggle to accurately depict thin geological layers, all while being constrained by limited vertical seismic resolution. Additionally, deterministic inversion methods are challenged by their inability to directly recover precise values of acoustic impedance from seismic traces due to band limitation.⁶⁹

A comparison between model-based seismic inversion (conventional) and ML-approximated acoustic impedance (integrating ResNet and CWT algorithms) is depicted in Figure 8a,b, respectively. The blocky nature of deterministic inverted property suggested the missing high-frequency components with only low-frequency incorporation through the LFM. The conventional inverted property is band-limited

in nature and tuned the thin sands of varied B-interval dispersed throughout the field. It clearly differentiated that layers refining are prominent in the ML-derived acoustic impedance. In both techniques, a good match of estimated volumetrics is observed at well locations by coloring wells with relevant properties, however, the layer resolution is comprehensively increased in ML property. The low-value ranges ($7500 \text{ m/s} \cdot \text{g/cm}^3$) encompassing the gas sands between shales demarcate the potential presence in the B-interval. As the resolution is enhanced and finer resolution is achieved, the ML property deals more thoroughly with the heterogeneities. The map of the ML-based P-impedance is depicted in Figure 9, which demarcated the channelized potential body passing through good gas-producing wells, i.e., Buzdar S_01 and Buzdar SD_03, along with limited production well of Buzdar SD_04. The blind wells, i.e., Buzdar S_02 and Buzdar SD_01,

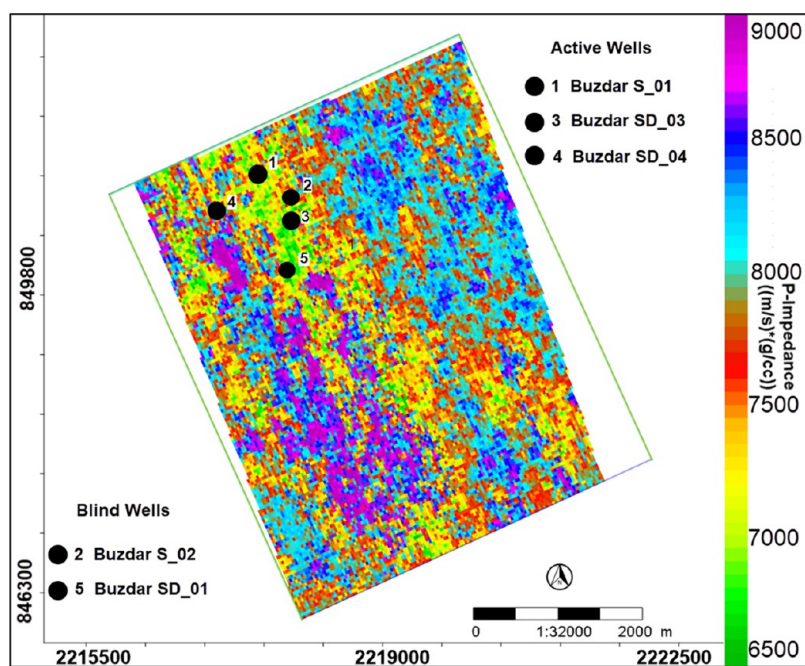


Figure 9. Average values within the B-interval depicted low impedances ($<7500 \text{ m/s}^2/\text{g/cm}^3$) for potential sand bodies.

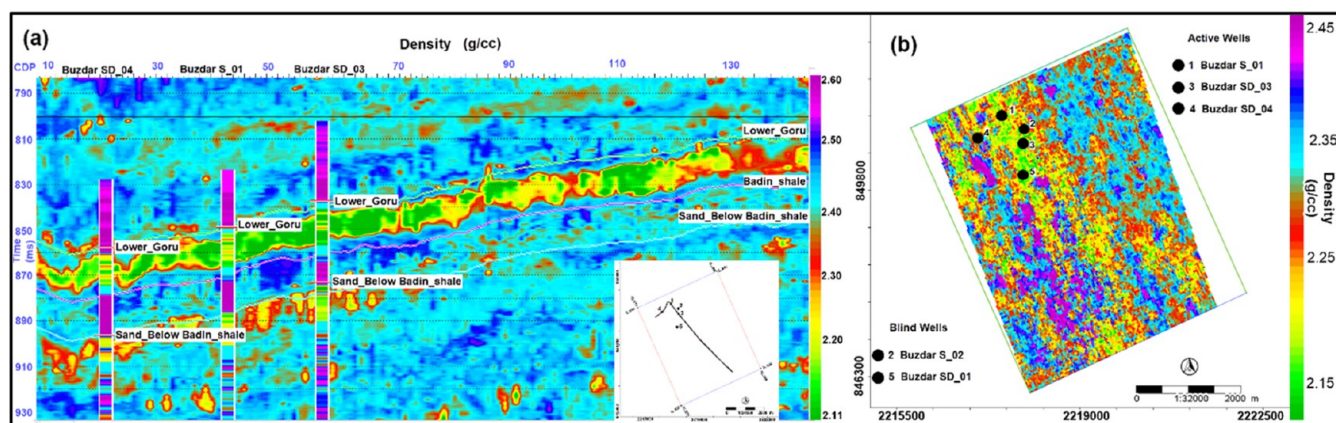


Figure 10. (a) RHOB displayed in section view through an arbitrary line delineating low-density sand bodies within the B-interval of the LGF and (b) the less dense body is passing through all of the wells (active and blind) while illustrating channelized sands throughout the field.

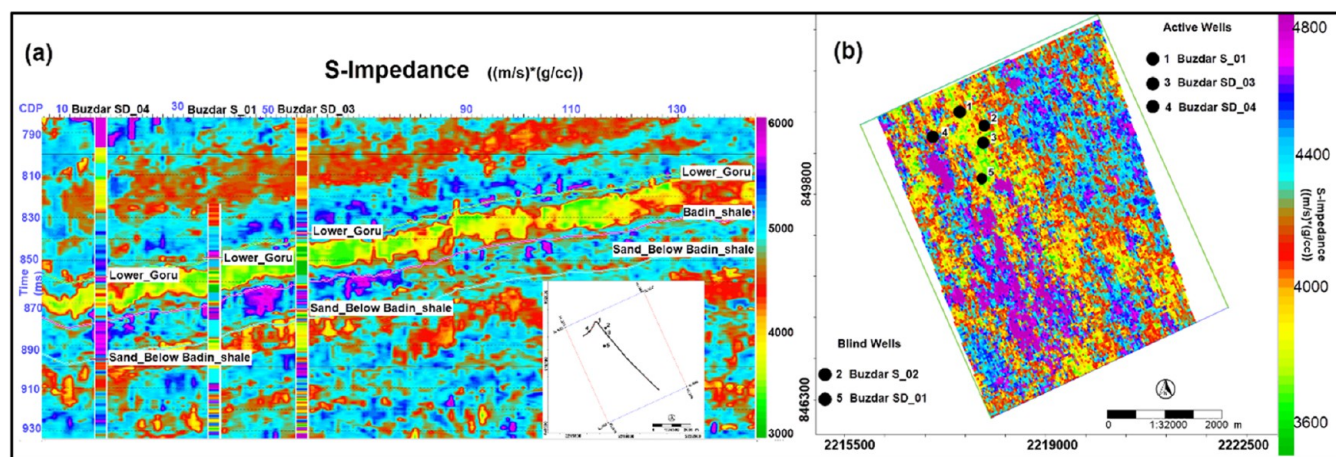


Figure 11. (a) Section of S-impedance demarcated the potential zone through specific value ranges ($<4000 \text{ m/s}^2/\text{g/cm}^3$) passing through wells colored with similar properties and (b) the map assessed the S-impedance throughout the field and captured similar trends of channelized potential body comparable to P-impedance.

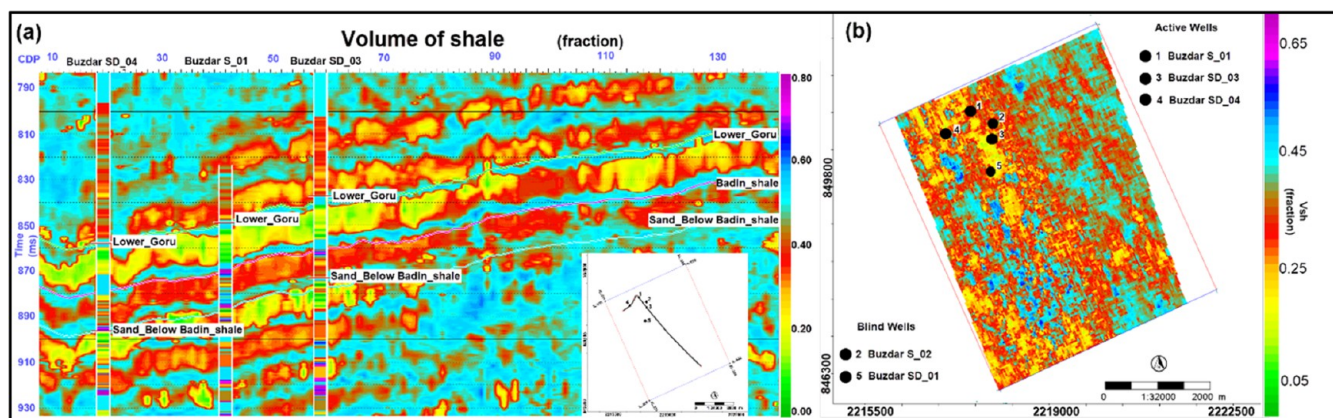


Figure 12. (a) Less Vsh is estimated within the B-interval sands of LGF with a decent match of wells and (b) Vsh map outlined less shaly content (<0.30) passing through wells while outlining additional promising zones.

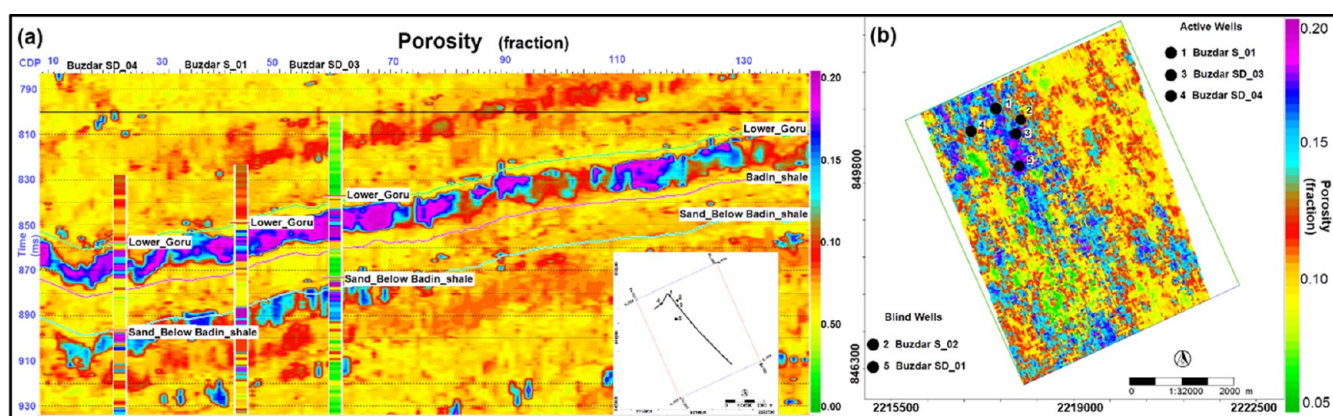


Figure 13. (a) High porosity is observed within B-interval sands passing through all wells and (b) the porosity distribution map highlighted porous zones feasible for entrapping gaseous fluids.

demonstrated low impedances, hence confirming their productivity.

The other important property, including the RHOB, is depicted on an arbitrary line in Figure 10a. The RHOB serves as a crucial indicator to validate the existence of less dense fluids. Low RHOB values i.e., 2.3 g/cm^3, are typically associated with the presence of fluid gas within rock formations.⁷⁰ Porous sand reservoirs containing hydrocarbons reduce the stiffness and hence reduce elastic properties, such as P-impedance, S-impedance, RHOB, and the V_p/V_s ratio. Low RHOB values suggest that the subsurface material is not very compact and contains porous materials with less dense fluids, mainly gas. The map of RHOB generated by taking the average values within reservoir B-sands exhibited low values for gas-prone sand bodies (Figure 10b). The low values in all three wells along with the blind wells confirm the presence of less dense sand bodies.⁷⁰

The product of RHOB and DTS is a vital property for confirming the fluids in the reservoir sands. The S-impedance is normally evaluated alongside the P-impedance for lithological as well as pore fluid identification.⁷⁰ Figure 11a depicts the S-impedance section bisecting wells and prominently demarcates the potentially important B-interval sand body. Below the major gas-bearing sand bed, a thin gas-prone bed is also present around the time (910 ms) passing through active wells and observed also in other elastic property sections, including P-impedance and RHOB. This thin bed can

be assessed as a future prospect of the field. The S-impedance is mapped within the B-interval and a very similar trend of the channelized gas-prone zone delineated through values ($4000 \text{ m/s}^2 \text{ g/cm}^3$) is observed throughout the field passing through active and blind wells (Figure 11b).

The estimation of petrophysical properties plays its part in elaborating the heterogeneities, regarding porosities, shale volumetrics, and fluid distribution, mainly water. The Vsh property displayed in the section through a similar arbitrary line demonstrated the presence of low shale contents in the B-interval (Figure 12a). Overall, clean sands are present at well locations with values less than 30%, while comparatively high shaly contents are observed in the southeastern portion. A decent tie is perceived among the modeled Vsh displayed in sections and wells that are colored with similar attributes. The Vsh mapping in the B-interval captured the variability regarding shale distribution throughout the field and depicted less quantities by supporting the results derived through elastic properties (Figure 12b).

One of the key petrophysical properties, i.e., PHIE is displayed in the section view bisecting well locations (Figure 13a). The wells are colored with similar properties and a good match is observed among PHIE volumetric and wells. Good porosity values are present at well locations in the B-interval ranging up to a maximum of 20%. For an obvious understanding, the porosity is mapped, which depicts porous channelized sand bodies that act as play fairways (Figure 13b).

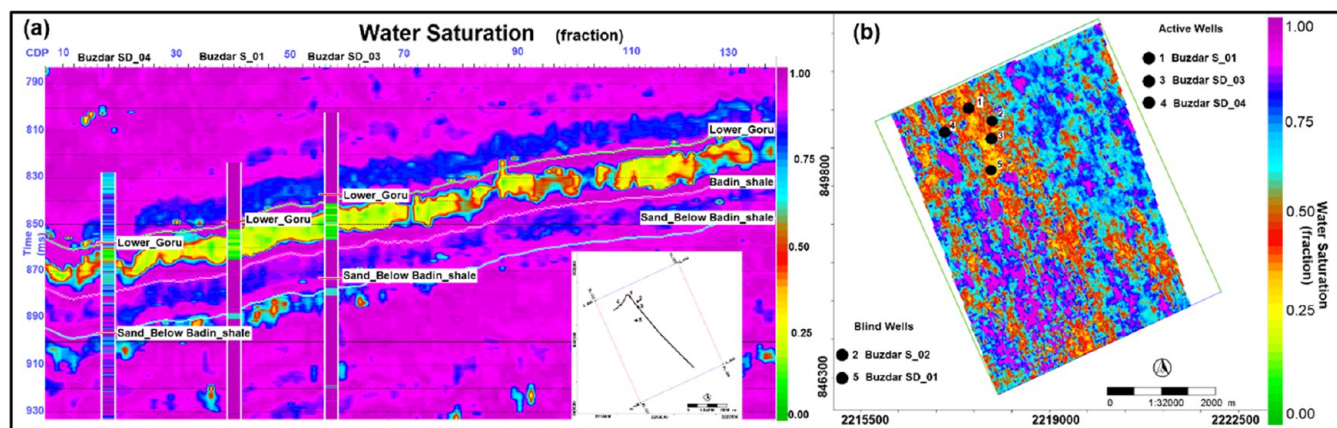


Figure 14. (a) Low Sw is present among all wells, clarifying the potential capability of B-interval, and (b) Sw is mapped as having low values at producing wells along with discrimination of plausible gas-prone sands.

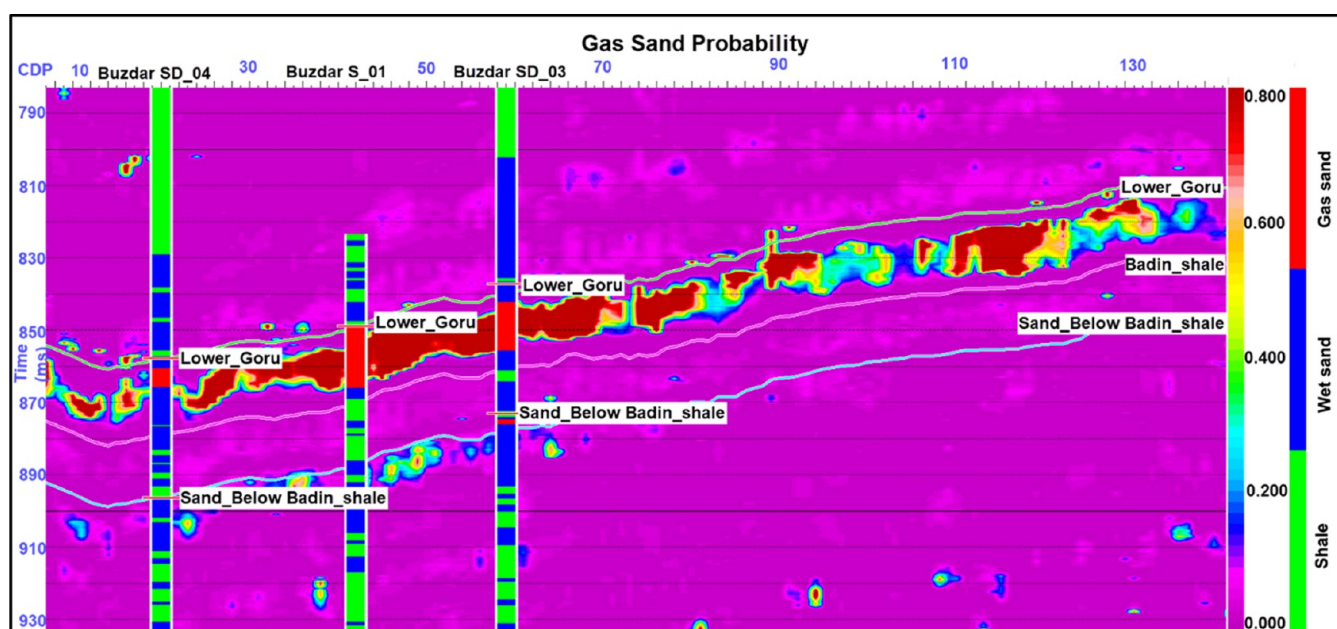


Figure 15. Decent match between wells and estimated gas sands is observed, while high gas sand probability is present in the B-interval sand.

Overall, there is diversity in the distribution of porosity in the field with the demarcation of compacted zones (porosity less than 5%), which are not feasible for additional wells.

The Sw is depicted in the section view, where low values (<0.45) are present at well locations within the B-interval (Figure 14a). The results obtained are too supportive among other petrophysical properties for the vibrant discrimination of clean, porous sands filled with gas. The Sw map also illuminated the sands with low water content throughout the field having average values of less than 50% in the B-interval (Figure 14b).

One of the key advantages is the approximation of the gas sand facies distribution utilizing the estimated Vsh, PHIE, and Sw. For gas sands, the Sw less than 45%, Vsh less than 30%, and PHIE greater than 5% are employed clearly distinguished producing sands as depicted on the section view (Figure 15a). High probability values at the B-interval are aligned with the identified gas-bearing sand facies at the well location. For the distribution of gas sands, the B-interval is mapped that justifies all of the results (elastic and petrophysical) and discriminates the producing sand bodies (Figure 16). The map demon-

strated high gas sand probability values and confirmed that the channelized sand body acts as a play fairway for the producing wells.

5. DISCUSSION

Seismic data can be affected by numerous factors, encompassing lithological variations, complexities in data acquisition, limitations in frequency bands, issues related to scale, and variations in both vertical and lateral sedimentary deposition.⁷¹ Nonetheless, when the hydrocarbon-bearing strata lie beneath the vertical resolution of seismic data, the task of characterizing the reservoir becomes notably more formidable.⁷² Comparable challenges were encountered in a research area in which the detection of heterogeneous thin prospective sands proved elusive when utilizing a data set having limitations among a limited frequency range of poststack seismic data. In this situation, not only did the conventional seismic data lack information regarding low-high frequency ranges but attempts to enhance its utility through deterministic inversion of poststack model-based inversion, focusing solely on low

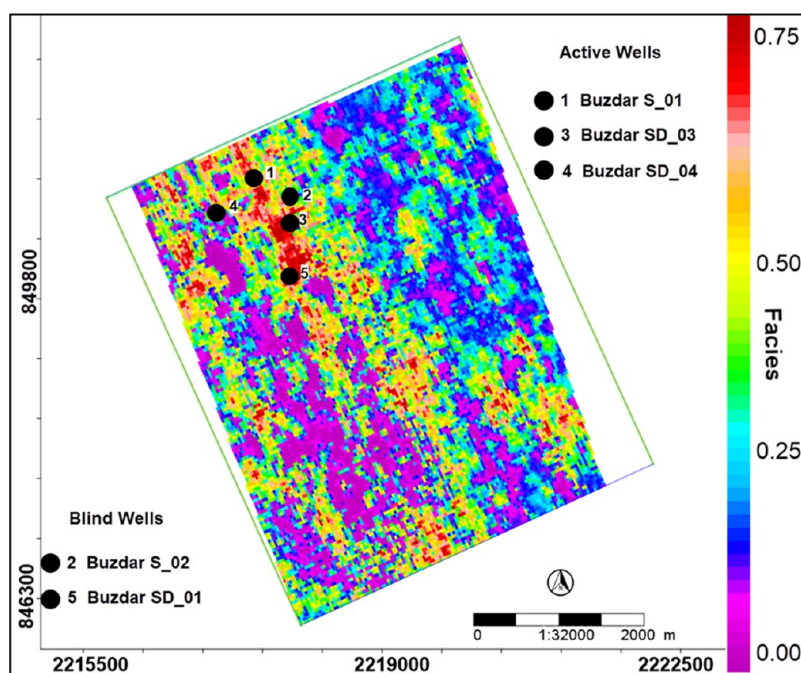


Figure 16. Integrated approach of ResNet and CWT modeled the probabilistic output of gas sands, illuminating the porous, gaseous, and channelized sand bodies.

frequencies, also proved unsuccessful in highlighting subtle geological features. This signifies the difficulty in accurately characterizing the reservoir on the band-limited seismic data set along with the unavailability of its multiangle ranges. The missing DTS also created a hurdle for building a petroelastic relationship that helps capture the complexity of the subsurface geology.⁷³

DTP and DTS play a vital role in building rock physics templates for the classification of lithofacies.^{74,75} Previously, to address the issues regarding DTP and DTS, linear relationships were taken among the seismic velocities and relevant rock properties, such as pores, fluids, shale volumetrics, etc., for assessing poor or missing zones.^{76–78} Contrarily, ML acts as an efficacious tool having the capability of building nonlinear relationships amid logs based on prominent features for unrecorded log estimation especially DTS that comprehensively appraise the reservoir characteristics. Due to the intricate reservoir properties of the B-interval along with the limitations in data, the ML techniques proved critical and acted as an enhanced tool for approximating the DTS.⁸ The accuracy of the estimated DTS is valued by statistical measures, including R2 and MAPE.⁷⁸ Few many researchers have successfully applied ML approaches for DTS prediction, i.e., Gamal et al.,¹² employed RF for building sonic prediction models in complex lithology rocks, including sandstone, limestone shale, and carbonate formations. In the study area, the most effective ML algorithm in predicting the missing DTS was DTS, identified through evaluation metrics applied to the different sample data sets extracted from training.

Recent studies conducted in the LGF sand intervals were performed to highlight the plausible gas-bearing sands.⁷⁹ Various authors performed multiple poststack inversion methods to calculate the reservoir parameters integrating seismic attributes, well logging, and inversion techniques.^{24,80,81} However, developing a novel approach incorporating wells and seismic for petroelastic relationships through

integration of ResNet and CWT provided comprehensive results for quantitative assessments of facies heterogeneity.

The CWT of seismic data serves as an effective technique for improving resolution capabilities and analyzing the stratigraphic units in more detail. Cumulatively, it encompasses the optimized hydrocarbon-bearing reservoir characterization, thickness estimation, stratigraphy imaging, and the successful exploration, and discovery of oil and gas resources.^{51,54,82} The researchers have proven the application of CWT along with conventional seismic inversion for sedimentological investigations assessing heterogeneities, including horizontal and vertical variability of facies and fluids.^{25,26} Advanced data analysis techniques, including signal processing (CWT) and DNN (ResNet), are employed to obtain robust, efficient, multicomponent outcomes on limited data sets for predicting elastic and petrophysical properties that gain thorough insights about the subsurface.

The classic neural networking (NN) approximation is adopted for handling various geophysical concerns, including wavelet calculations,⁵⁵ velocity investigation,⁸³ autopick of horizons,⁸⁴ lithofacies classification on seismic,^{85–87} and for the relationship of seismic extracted attributes toward their reservoir characteristics.⁸⁸ However, notwithstanding its numerous effective procedures in exploration geophysics, the classic NN method has severe restrictions and shortcomings. In specific, the NN method is chiefly limited by its gradient-based nature.⁸⁹ ResNet is a DNN architecture that has gained recognition for its proficiency in effectively managing exceptionally deep networks. Its composition encompasses multiple layers, encompassing convolutional layers, residual blocks, and fully connected layers.⁶²

The integration of CWT and the ResNet architecture brings together the advantages of the robust learning capabilities of DNN. This innovative method has the potential to significantly enhance the precision and effectiveness of subsurface characterization, making it extremely beneficial in the oil and

gas industry. It plays a pivotal role in optimizing reservoir evaluation and exploration activities.

Low P-impedance of the studied field acknowledged gas-prone sand lithologies encased between shaly compartments having comparatively higher values due to their compactness and stiffness.⁹⁰ The low-value ranges (less than 7000 m/s²*g/cm³) of P-impedances are also observed in nearby gas-producing fields for thin heterogeneous potential sand intervals of the LGF, including Kadanwari, Mubarak, Rehmat, etc., using conventional procedures. The exact values of thin heterogeneous Khadro Formation of the LIB are successfully observed through the conventional technique of stochastic inversion after following a detailed and multistep process.⁹¹ Similarly, S-impedance obtained through advanced ML integrated techniques followed trends that strengthened P-impedance outcomes with low values, illuminating gas-filled sands. S-impedances approximated through conventional algorithms played their role by providing valuable information regarding fluids, including Zamzama and Rehmat gas fields.^{6,7,24}

The main geological factors that introduce the heterogeneity effects include porosity, shale contents, and fluids.²⁴ These properties are comprehensively assessed in the research area, and their variability is demarcated throughout the field. The low Vsh values (less than 30%) along with high Vsh values (10–15%) indicate prominent reservoirs of the LIB.^{92,93} Overall, low Vsh and high PHIE with low Sw are observed in the study area, which clarifies the distribution of the B-interval channelized sand body in the study area, which is more pronouncedly delineated by the facies distribution mapping. Good portions of potential capabilities are observed in the field that can be tested for additional wells and enhanced production from the field.

6. CONCLUSIONS

Numerous goals have been accomplished, beginning with overcoming data restrictions by precisely predicting missing DTS in all wells through ML algorithms. Limitation of low-resolution seismic for characterizing thin sand had been attained by developing a novel approach, i.e., an integrating advanced ML technique (ResNet) with decomposed seismic traces of CWT. The incorporation of multiscale properties through the employed technique has the potential to revolutionize subsurface properties through the approximation of enhanced elastic and petrophysical attributes, benefiting hydrocarbon exploration and production efforts. The elastic attributes (P-impedance <7500 m/s²*g/cm³, S-impedance <4000 m/s²*g/cm³, RHOB < 2.3 g/cm³) and the petrophysical properties, such as Vsh < 0.3, PHIE ≈ 20, and Sw < 0.45, successfully demarcated the thin channelized sand body throughout the field along with the incorporation of the heterogeneities. Risk-efficient potential zones have been designated that can be drilled for optimized production of the field. Hence, the cost-effective, time-efficient, and less laborious techniques successfully handled major data limitations with improved property extraction for accurate characterization of thin potential heterogeneous bodies.

AUTHOR INFORMATION

Corresponding Author

Saima Akram – Department of Earth Sciences, Quaid-I-Azam University, Islamabad 45320, Pakistan;  orcid.org/0009-0009-4001-9981; Email: saimaakram@geo.qau.edu.pk

Authors

Gulraiz Akhter – Department of Earth Sciences, Quaid-I-Azam University, Islamabad 45320, Pakistan

Yonggang Ge – Institute of Mountain Hazards and Environment, Chinese Academy of Sciences, Chengdu 610041, China; Key Laboratory of Mountain Hazards and Earth Surface Processes, Chinese Academy of Sciences, Chengdu 610041, China

Tahir Azeem – Department of Earth Sciences, Quaid-I-Azam University, Islamabad 45320, Pakistan

Complete contact information is available at:

<https://pubs.acs.org/10.1021/acsomega.3c08169>

Notes

The authors declare no competing financial interest.

ACKNOWLEDGMENTS

The authors would like to thank the Directorate General of Petroleum Concessions (DGPC) for providing the data. They are also thankful to the Reservoir Characterization Department of LMKR, Islamabad, and CGG Geosoft for their cooperation regarding technical and software support. The research was financially supported by the International Science & Technology Cooperation Program of China, grant number 2018YFE0100100.

REFERENCES

- (1) Munir, K.; Iqbal, M. A.; Farid, A.; Shabih, S. M. Mapping the Productive Sands of Lower Goru Formation by Using Seismic Stratigraphy and Rock Physical Studies in Sawan Area, Southern Pakistan: A Case Study. *J. Pet. Explor. Prod. Technol.* **2011**, *1*, 33–42.
- (2) Munir, A.; Asim, S.; Bablani, S. A.; Asif, A. A. Seismic Data Interpretation and Fault Mapping in Badin Area, Sindh, Pakistan *Sindh University Research Journal-SURJ (Science Series)* **2014**; Vol. 46 *2*, pp 133–142.
- (3) Yar, M.; Haider, S. W.; Nabi, G.; Tufail, M.; Rahman, S. Reservoir Characterization of Sand Intervals of Lower Goru Formation Using Petrophysical Studies; A Case Study of Zaur-03 Well, Badin Block, Pakistan. *Int. J. Econ. Environ. Geol.* **2019**, *10* (3), 118–124.
- (4) Nisar, U. B.; Rizwan, M.; Khan, M. R.; Farooq, M.; Qureshi, S. N.; Ahmed, K. A. Identification of Sealing Potential through Fault Seal Analysis: A Case Study of Badin Area, Lower Indus Basin, Pakistan. *Geofis. Int.* **2019**, *58* (2), 139–150, DOI: [10.22201/igeof.00167169p.2018.58.2.1966](https://doi.org/10.22201/igeof.00167169p.2018.58.2.1966).
- (5) Rashad, O.; El-Barkooky, A. N.; El-Araby, A.; El-Tonbary, M. Deterministic and Stochastic Seismic Inversion Techniques towards a Better Prediction for the Reservoir Distribution in NEAG-2 Field, North Western Desert, Egypt. *Egypt. J. Pet.* **2022**, *31* (1), 15–23.
- (6) Hussain, M.; Khan, Z. U.; Ahmed, S. A. Quantifying Thin Heterogeneous Gas Sand Facies of Rehmat Gas Field by Developing Petro Elastic Relationship in Fine Stratigraphic Layers through Bayesian Stochastic Seismic Inversion. *Mar. Pet. Geol.* **2023**, *149*, No. 106074.
- (7) Shakir, U.; Ali, A.; Amjad, M. R.; Hussain, M. Improved Gas Sand Facies Classification and Enhanced Reservoir Description Based on Calibrated Rock Physics Modelling: A Case Study. *Open Geosci.* **2021**, *13* (1), 1476–1493.
- (8) Ahmed, S. A.; Hussain, M.; Khan, Z. U. Supervised Machine Learning for Predicting Shear Sonic Log (DTS) and Volumes of Petrophysical and Elastic Attributes, Kadanwari Gas Field, Pakistan. *Front. Earth Sci.* **2022**, *10*, No. 919130.
- (9) Azeem, T.; Chun, W. Y.; MonaLisa; Khalid, P.; Qing, L. X.; Ehsan, M. I.; Munawar, M. J.; Wei, X. An Integrated Petrophysical and Rock Physics Analysis to Improve Reservoir Characterization of

- Cretaceous Sand Intervals in Middle Indus Basin, Pakistan. *J. Geophys. Eng.* **2017**, *14* (2), 212–225.
- (10) Wawrzyniak-Guz, K. Rock Physics Modelling for Determination of Effective Elastic Properties of the Lower Paleozoic Shale Formation, North Poland. *Acta Geophys.* **2019**, *67* (6), 1967–1989.
- (11) Bukar, I.; Adamu, M. B.; Hassan, U. A Machine Learning Approach to Shear Sonic Log Prediction. In *SPE Nigeria Annual International Conference and Exhibition*; OnePetro, 2019.
- (12) Gamal, H.; Alsaihati, A.; Elkatatny, S. Predicting the Rock Sonic Logs While Drilling by Random Forest and Decision Tree-Based Algorithms. *J. Energy Resour. Technol.* **2022**, *144* (4), No. 043203, DOI: [10.1115/1.4051670](https://doi.org/10.1115/1.4051670).
- (13) Liu, S.; Zhao, Y.; Wang, Z. Artificial Intelligence Method for Shear Wave Travel Time Prediction Considering Reservoir Geological Continuity. *Math. Probl. Eng.* **2021**, *2021*, 1–18.
- (14) Miah, M. I. Improved Prediction of Shear Wave Velocity for Clastic Sedimentary Rocks Using Hybrid Model with Core Data. *J. Rock Mech. Geotech. Eng.* **2021**, *13* (6), 1466–1477.
- (15) Naseer, M. T. Seismic Attributes and Quantitative Stratigraphic Simulation'application for Imaging the Thin-Bedded Incised Valley Stratigraphic Traps of Cretaceous Sedimentary Fairway, Pakistan. *Mar. Pet. Geol.* **2021**, *134*, No. 105336.
- (16) Davarpanah, A. Parametric Study of Polymer-Nanoparticles-Assisted Injectivity Performance for Axisymmetric Two-Phase Flow in EOR Processes. *Nanomaterials* **2020**, *10* (9), 1818.
- (17) Davarpanah, A.; Mirshekari, B.; Jafari Behbahani, T.; Hemmati, M. Integrated Production Logging Tools Approach for Convenient Experimental Individual Layer Permeability Measurements in a Multi-Layered Fractured Reservoir. *J. Pet. Explor. Prod. Technol.* **2018**, *8*, 743–751, DOI: [10.1007/s13202-017-0422-3](https://doi.org/10.1007/s13202-017-0422-3).
- (18) Hu, X.; Xie, J.; Cai, W.; Wang, R.; Davarpanah, A. Thermodynamic Effects of Cycling Carbon Dioxide Injectivity in Shale Reservoirs. *J. Pet. Sci. Eng.* **2020**, *195*, No. 107717.
- (19) Miao, X.; Todorovic-Marinic, D.; Klatt, T. Enhancing Seismic Insight by Spectral Decomposition. In *SEG International Exposition and Annual Meeting*; SEG, 2007; p SEG-2007.
- (20) Sharma, R.; Reddy, K.; Josyula, S. Application of Continuous Wavelet Transformation (CWT) and Time Frequency Wavelet Transformation (TFCWT) for Improved Temporal Resolution of Thin Beds-A Case Study.
- (21) Haris, A.; Haryono, H.; Riyanto, A. Spectral Decomposition Technique Based On Stft And Cwt For Identifying The Hydrocarbon Reservoir. *Sci. Contrib. Oil and Gas* **2018**, *40* (3), 125–131.
- (22) Sinaga, T. M.; Rosid, M. S.; Haidar, M. W. Porosity Prediction Using Neural Network Based on Seismic Inversion and Seismic Attributes. In *E3S Web of Conferences*; EDP Sciences, 2019; p 15006.
- (23) Durrani, M. Z. A.; Talib, M.; Ali, A.; Sarosh, B.; Naseem, N. Characterization and Probabilistic Estimation of Tight Carbonate Reservoir Properties Using Quantitative Geophysical Approach: A Case Study from a Mature Gas Field in the Middle Indus Basin of Pakistan. *J. Pet. Explor. Prod. Technol.* **2020**, *10* (7), 2785–2804, DOI: [10.1007/s13202-020-00942-0](https://doi.org/10.1007/s13202-020-00942-0).
- (24) Khan, Z. U.; Lisa, M.; Hussain, M.; Ahmed, S. A. Gas-Bearing Sands Appraisal for Zamzama Gas Field in Pakistan through Inverted Elastic Attributes Assisted with PNN Approximation of Petrophysical Properties *Kuwait J. Sci.* **2022**; Vol. 49 4.
- (25) Suarez, Y.; Marfurt, K. J.; Falk, M. Seismic Attribute-Assisted Interpretation of Channel Geometries and Infill Lithology: A Case Study of Anadarko Basin Red Fork Channels. In *SEG Technical Program Expanded Abstracts 2008*; Society of Exploration Geophysicists, 2008; pp 963–967.
- (26) Wei, X.; Wang, X.; Yanqing, Z.; Cai, J.; Yongmei, S. Application of Spectral Decomposition in Hydrocarbon Detection. In *SEG International Exposition and Annual Meeting*; SEG, 2011; p SEG-2011.
- (27) Sang, W.; Ding, Z.; Li, M.; Liu, X.; Liu, Q.; Yuan, S. Prestack Simultaneous Inversion of P-Wave Impedance and Gas Saturation Using Multi-Task Residual Networks. *Acta Geophys.* **2023**, 1–18.
- (28) Alom, M. Z.; Taha, T. M.; Yakopcic, C.; Westberg, S.; Sidike, P.; Nasrin, M. S.; Hasan, M.; Van Essen, B. C.; Awwal, A. A.; Asari, V. K. A State-of-the-Art Survey on Deep Learning Theory and Architectures. *Electronics* **2019**, *8* (3), 292.
- (29) Otter, D. W.; Medina, J. R.; Kalita, J. K. A Survey of the Usages of Deep Learning for Natural Language Processing. *IEEE Trans. Neural Networks and Learning Syst.* **2021**, *32* (2), 604–624.
- (30) Dawson, H. L.; Dubrule, O.; John, C. M. Impact of Dataset Size and Convolutional Neural Network Architecture on Transfer Learning for Carbonate Rock Classification. *Comput. Geosci.* **2023**, *171*, No. 105284.
- (31) Koeshidayatullah, A.; Al-Azani, S.; Baraboshkin, E. E.; Alfarraj, M. Faciesvit: Vision Transformer for an Improved Core Lithofacies Prediction. *Front. Earth Sci.* **2022**, *10*, No. 992442.
- (32) Zhang, W.; Li, H.; Li, Y.; Liu, H.; Chen, Y.; Ding, X. Application of Deep Learning Algorithms in Geotechnical Engineering: A Short Critical Review. *Artif. Intell. Rev.* **2021**, *54*, 1–41, DOI: [10.1007/s10462-021-09967-1](https://doi.org/10.1007/s10462-021-09967-1).
- (33) Alam, M. S. M.; Wasimuddin, M.; Ahmad, S. S.Zaur Structure, A Complex Trap in a Poor Seismic Data Area. In *BP Pakistan Exploration & Production Inc. Annu. Tech. Conf.(ATC)* Islamabad, Pakistan, 2002; pp 2–4.
- (34) Naeem, M.; Jafri, M. K.; Moustafa, S. S.; AL-Arifi, N. S.; Asim, S.; Khan, F.; Ahmed, N. Seismic and Well Log Driven Structural and Petrophysical Analysis of the Lower Goru Formation in the Lower Indus Basin, Pakistan. *Geosci. J.* **2016**, *20*, 57–75.
- (35) Farah, A.; Abbas, G.; De Jong, K. A.; Lawrence, R. D. Evolution of the Lithosphere in Pakistan. *Tectonophysics* **1984**, *105* (1–4), 207–227.
- (36) Kadri, I. B. Petroleum Geology of Pakistan: Pakistan Petroleum Limited *Karachi, Pakistan* 1995.
- (37) Gnos, E.; Immenhauser, A.; Peters, T. J. Late Cretaceous/Early Tertiary Convergence between the Indian and Arabian Plates Recorded in Ophiolites and Related Sediments. *Tectonophysics* **1997**, *271* (1–2), 1–19.
- (38) Ahmed, S.; Solangi, S. H.; Jadoon, M. S. K.; Nazeer, A. Tectonic Evolution of Structures in Southern Sindh Monocline, Indus Basin, Pakistan Formed in Multi-Extensional Tectonic Episodes of Indian Plate. *Geod. Geodyn.* **2018**, *9* (5), 358–366, DOI: [10.1016/j.geog.2018.03.004](https://doi.org/10.1016/j.geog.2018.03.004).
- (39) Besse, J.; Courtillot, V. Paleogeographic Maps of the Continents Bordering the Indian Ocean since the Early Jurassic. *J. Geophys. Res.: Solid Earth* **1988**, *93* (B10), 11791–11808.
- (40) Ebdon, C.; Wasimuddin, M.; Malik, A. H.; Akhter, S. Sequence Stratigraphy of the B Sand (Upper Sand, Lower Goru Formation) in the Badin Area: Implication for Development and Exploitation. In *Annu. Tech. Conf.* Islamabad, Pakistan, 2004.
- (41) Porth, H.; Raza, H. A. The Geology and Hydrocarbon Prospects of Sulaiman Province *Indus Basin Pakistan* 1990.
- (42) Ahmad, N.; Mateen, J.; Chaudry, K. S.; Mehmood, N.; Arif, F. Shale Gas Potential of Lower Cretaceous Sembar Formation in Middle and Lower Indus Basin, Pakistan. *Pak. J. Hydrocarbon Res.* **2013**, *23*, 51–62.
- (43) Ahmad, S.; Ghazi, S. Depositional Trends and Reservoir Geometries of the Early Cretaceous Lower Goru Formation in Lower Indus Basin, Pakistan: Evidence from Sequence Stratigraphy. *J. Pet. Explor. Prod. Technol.* **2022**, *12* (11), 2981–3001, DOI: [10.1007/s13202-022-01489-y](https://doi.org/10.1007/s13202-022-01489-y).
- (44) Sychala, Y. T.; Ramaaker, T. A.; Eggenhuisen, J. T.; Grundvåg, S.-A.; Pohl, F.; Wróblewska, S. Proximal to Distal Grain-size Distribution of Basin-floor Lobes: A Study from the Battfjället Formation, Central Tertiary Basin, Svalbard. *Depositional Rec.* **2022**, *8* (2), 436–456, DOI: [10.1002/dep2.167](https://doi.org/10.1002/dep2.167).
- (45) Kazmi, A. H.; Snee, L. W. Geology of World Emerald Deposits: A Brief Review. *Emeralds of Pakistan. Geol., Gemol. Genesis* **1989**, 165–228, DOI: [10.1007/978-1-4899-5826-6_8](https://doi.org/10.1007/978-1-4899-5826-6_8).
- (46) Abbasi, S. A.; Kalwar, Z.; Solangi, S. H. Study of Structural Styles and Hydrocarbon Potential of RajanPur Area, Middle Indus Basin, Pakistan. *Bu J. ES* **2016**, *1* (1), 36–41.

- (47) Wicaksono, T.; Haris, A.; Riyanto, A.; Riyadi, P. Reservoir Characterization Using Stochastic Seismic Inversion in “K” Gas Field, Bonaparte Basin. In *AIP Conference Proceedings*; AIP Publishing, 2021.
- (48) Lijtens, G.; Kooi, T.; Bejnordi, B. E.; Setio, A. A. A.; Ciompi, F.; Ghafoorian, M.; Van Der Laak, J. A.; Van Ginneken, B.; Sánchez, C. I. A Survey on Deep Learning in Medical Image Analysis. *Med. Image Anal.* **2017**, *42*, 60–88, DOI: 10.1016/j.media.2017.07.005.
- (49) Manzoor, U.; Ehsan, M.; Hussain, M.; Iftikhar, M. K.; Abdelrahman, K.; Qadri, S. T.; Arshad, F.; Ashraf, K.; Fnais, M. S. Harnessing Advanced Machine-Learning Algorithms for Optimized Data Conditioning and Petrophysical Analysis of Heterogeneous, Thin Reservoirs. *Energy Fuels* **2023**, *37* (14), 10218–10234.
- (50) McDonald, A. Data Quality Considerations for Petrophysical Machine-Learning Models. *Petrophysics* **2021**, *62* (06), 585–613.
- (51) Naseer, M. T.; Asim, S. Continuous Wavelet Transforms of Spectral Decomposition Analyses for Fluvial Reservoir Characterization of Miano Gas Field, Indus Platform, Pakistan. *Arabian J. Geosci.* **2017**, *10*, No. 210, DOI: 10.1007/s12517-017-2920-5.
- (52) Sinha, S.; Routh, P. S.; Anno, P. D.; Castagna, J. P. Spectral Decomposition of Seismic Data with Continuous-Wavelet Transform. *Geophysics* **2005**, *70* (6), P19–P25.
- (53) Mallat, S. *A Wavelet Tour of Signal Processing*; Elsevier, 1999.
- (54) Li, W.; Yue, D.; Wang, W.; Wang, W.; Wu, S.; Li, J.; Chen, D. Fusing Multiple Frequency-Decomposed Seismic Attributes with Machine Learning for Thickness Prediction and Sedimentary Facies Interpretation in Fluvial Reservoirs. *J. Pet. Sci. Eng.* **2019**, *177*, 1087–1102.
- (55) Wang, J.; Tan, X.; Tian, J.; Luo, L.; Gao, X.; Luo, C.; Zeng, C.; Zhang, L.; Xue, W. The Effect of Diagenetic Evolution on Shale Gas Exploration and Development of the Longmaxi Formation Shale, Sichuan Basin, China. *Front. Earth Sci.* **2021**, *9*, No. 661581.
- (56) Sudarmaji, M.; Sismanto, M.; Waluyo, M. Estimation of Frequency Dependent Attenuation of Seismic Wave in Time-Frequency Domain Based on Continuous Wavelet Transform (CWT). In *International Conference on Physics 2014 (ICP-14)*; Atlantis Press, 2014; pp 68–73.
- (57) Polikar, R. *The Wavelet Tutorial*; 1996.
- (58) Selesnick, I. W.; Baraniuk, R. G.; Kingsbury, N. C. The Dual-Tree Complex Wavelet Transform. *IEEE Signal Process. Mag.* **2005**, *22* (6), 123–151, DOI: 10.1109/MSP.2005.1550194.
- (59) Kanfar, R.; Shaikh, O.; Yousefzadeh, M.; Mukerji, T. Real-Time Well Log Prediction from Drilling Data Using Deep Learning. In *International Petroleum Technology Conference*; IPTC, 2020D031S064R003.
- (60) Wawrzyniak, K. Application of Time-Frequency Transforms to Processing of Full Waveforms from Acoustic Logs. *Acta Geophys.* **2010**, *58*, 49–82.
- (61) Dramsch, J. S. 70 Years of Machine Learning in Geoscience in Review. *Adv. Geophys.* **2020**, *61*, 1–55.
- (62) Alzubaidi, L.; Zhang, J.; Humaidi, A. J.; Al-Dujaili, A.; Duan, Y.; Al-Shamma, O.; Santamaría, J.; Fadhel, M. A.; Al-Amidie, M.; Farhan, L. Review of Deep Learning: Concepts, CNN Architectures, Challenges, Applications, Future Directions. *J. Big Data* **2021**, *8*, 1–74.
- (63) Teuwen, J.; Moriakov, N. Convolutional Neural Networks. In *Handbook of Medical Image Computing and Computer Assisted Intervention*; Elsevier, 2020; pp 481–501.
- (64) Zaeemzadeh, A.; Rahnavard, N.; Shah, M. Norm-Preservation: Why Residual Networks Can Become Extremely Deep? *IEEE Trans. Pattern Anal. Mach. Intell.* **2021**, *43* (11), 3980–3990, DOI: 10.1109/TPAMI.2020.2990339.
- (65) Gao, M.; Song, P.; Wang, F.; Liu, J.; Mandelis, A.; Qi, D. A Novel Deep Convolutional Neural Network Based on ResNet-18 and Transfer Learning for Detection of Wood Knot Defects. *J. Sens.* **2021**, *2021*, 1–16.
- (66) Ahmad Fuad, M. I.; Hermana, M.; Jaya, M. S.; Ishak, M. A. A New Robust Weak Supervision Deep Learning Approach for Reservoir Properties Prediction in Malaysian Basin Field. *Appl. Sci.* **2023**, *13* (15), 9025.
- (67) Sinha, S. Statistical and Deep Learning Methods for Geoscience Problems. 2021.
- (68) Iraj, S.; Soltanmohammadi, R.; Matheus, G. F.; Basso, M.; Vidal, A. C. Application of Unsupervised Learning and Deep Learning for Rock Type Prediction and Petrophysical Characterization Using Multi-Scale Data. *Geoenergy Sci. Eng.* **2023**, *230*, No. 212241.
- (69) Ansari, H. R.; Motafakkerfard, R.; Riahi, M. A. Comparing Geostatistical Seismic Inversion Based on Spectral Simulation with Deterministic Inversion: A Case Study. *Iran. J. Oil Gas Sci. Technol.* **2014**, *3* (1), 1–14, DOI: 10.22050/ijogst.2014.5796.
- (70) Das, B.; Chatterjee, R. Well Log Data Analysis for Lithology and Fluid Identification in Krishna-Godavari Basin, India. *Arabian J. Geosci.* **2018**, *11*, No. 231, DOI: 10.1007/s12517-018-3587-2.
- (71) Mahmood, M. F.; Ahmad, Z.; Ehsan, M. Total Organic Carbon Content and Total Porosity Estimation in Unconventional Resource Play Using Integrated Approach through Seismic Inversion and Well Logs Analysis within the Talhar Shale, Pakistan. *J. Nat. Gas Sci. Eng.* **2018**, *52*, 13–24, DOI: 10.1016/j.jngse.2018.01.016.
- (72) Babasafari, A. A.; Ghosh, D. P.; Salim, A. M.; Kordi, M. Integrating Petroelastic Modeling, Stochastic Seismic Inversion, and Bayesian Probability Classification to Reduce Uncertainty of Hydrocarbon Prediction: Example from Malay Basin. *Interpretation* **2020**, *8* (3), SM65–SM82.
- (73) Xiang, L. M.; Lubis, L. A. Application of Simultaneous Inversion Characterizing Reservoir Properties in X Field, Sabah Basin. In *IOP Conference Series: Earth and Environmental Science*; IOP Publishing, 2017012022.
- (74) Avseth, P.; van Wijngaarden, A.-J.; Flesche, H.; Fristad, T.; Rykkje, J.; Mavko, G. Seismic Fluid Prediction in Poorly Consolidated and Clay Laminated Sands. In *67th EAGE Conference & Exhibition*; European Association of Geoscientists & Engineers, 2005; p cp-1.
- (75) Dvorkin, J.; Gutierrez, M. A.; Grana, D. *Seismic Reflections of Rock Properties*; Cambridge University Press, 2014.
- (76) Castagna, J. P.; Backus, M. M. *Offset-Dependent Reflectivity—Theory and Practice of AVO Analysis*; Society of Exploration Geophysicists, 1993.
- (77) Zorasi, C. B. Petrophysical and Geomechanical Characterization of a Marginal (Wabi) Field Reservoir in North-Central Niger Delta, Doctoral Dissertation; 2019.
- (78) Saad, B.; Negara, A.; Syed Ali, S. Digital Rock Physics Combined with Machine Learning for Rock Mechanical Properties Characterization. In *Abu Dhabi International Petroleum Exhibition and Conference*; SPE, 2018D011S008R001.
- (79) Ashraf, U.; Zhu, P.; Yasin, Q.; Anees, A.; Imraz, M.; Mangi, H. N.; Shakeel, S. Classification of Reservoir Facies Using Well Log and 3D Seismic Attributes for Prospect Evaluation and Field Development: A Case Study of Sawan Gas Field, Pakistan. *J. Pet. Sci. Eng.* **2019**, *175*, 338–351.
- (80) Ali, A.; Alves, T. M.; Saad, F. A.; Ullah, M.; Toqeer, M.; Hussain, M. Resource Potential of Gas Reservoirs in South Pakistan and Adjacent Indian Subcontinent Revealed by Post-Stack Inversion Techniques. *J. Nat. Gas Sci. Eng.* **2018**, *49*, 41–55, DOI: 10.1016/j.jngse.2017.10.010.
- (81) Yasin, Q.; Sohail, G. M.; Ding, Y.; Ismail, A.; Du, Q. Estimation of Petrophysical Parameters from Seismic Inversion by Combining Particle Swarm Optimization and Multilayer Linear Calculator. *Nat. Resour. Res.* **2020**, *29*, 3291–3317, DOI: 10.1007/s11053-020-09641-3.
- (82) Shahbazi, A.; Monfared, M. S.; Thiruchelvam, V.; Fei, T. K.; Babasafari, A. A. Integration of Knowledge-Based Seismic Inversion and Sedimentological Investigations for Heterogeneous Reservoir. *J. Asian Earth Sci.* **2020**, *202*, No. 104541.
- (83) Calderón-Macas, C.; Sen, M. K.; Stoffa, P. L. Automatic NMO Correction and Velocity Estimation by a Feedforward Neural Network. *Geophysics* **1998**, *63* (5), 1696–1707.
- (84) Huang, K.-Y.; Yang, J.-R. Seismic Velocity Picking Using Hopfield Neural Network. In *SEG International Exposition and Annual Meeting*; SEG, 2015; p SEG-2015.

(85) Coléou, T.; Poupon, M.; Azbel, K. Unsupervised Seismic Facies Classification: A Review and Comparison of Techniques and Implementation. *Leading Edge* **2003**, *22* (10), 942–953.

(86) Herrera, V. M.; Russell, B.; Flores, A. Neural Networks in Reservoir Characterization. *Leading Edge* **2006**, *25* (4), 402–411.

(87) Marroquín, I. D.; Brault, J.-J.; Hart, B. S. A Visual Data-Mining Methodology for Seismic Facies Analysis: Part 1—Testing and Comparison with Other Unsupervised Clustering Methods. *Geophysics* **2009**, *74* (1), P1–P11.

(88) Dorrington, K. P.; Link, C. A. Genetic-Algorithm/Neural-Network Approach to Seismic Attribute Selection for Well-Log Prediction. *Geophysics* **2004**, *69* (1), 212–221.

(89) Saggaf, M. M.; Toksöz, M. N.; Marhoon, M. I. Seismic Facies Classification and Identification by Competitive Neural Networks. *Geophysics* **2003**, *68* (6), 1984–1999.

(90) Ahmed, S. A.; Hussain, M.; Khan, Z. U. The Application of the PNN Algorithm to Evaluate the Petrophysical Properties of the Heterogeneous E-Sand Reservoirs, Lower Goru Formation, Pakistan. *Kuwait J. Sci.* **2023**, *50* (4), 773–782, DOI: [10.1016/j.kjs.2023.02.032](https://doi.org/10.1016/j.kjs.2023.02.032).

(91) Khan, Z. U.; Hussain, M.; Ahmed, S. A. Bayesian Stochastic Inversion with Petro-Elastic Relation to Quantify Thin Gas Sands of Khadro Formation, Zamzama Gas Field. *Episodes J. Int. Geosci.* **2023**, *46* (3), 389–405, DOI: [10.18814/epiiugs/2022/022039](https://doi.org/10.18814/epiiugs/2022/022039).

(92) Munir, M. N.; Zafar, M.; Ehsan, M. Comparative and Statistical Analysis of Core-Calibrated Porosity with Log-Derived Porosity for Reservoir Parameters Estimation of the Zamzama GAS Field, Southern Indus Basin, Pakistan. *Arabian J. Sci. Eng.* **2023**, *48* (6), 7867–7882.

(93) Siyar, S. M.; Waqas, M.; Mehmood, S.; Jan, A.; Awais, M.; Islam, F. Petrophysical Characteristics of Lower Goru Formation (Cretaceous) in Sawan Gas Field, Central Indus Basin, Pakistan. *J. Biol. Environ. Sci.* **2017**, *10* (5), 260–266.